José Maria Duque Neves Gouveia Fernandes

Licenciado em Engenharia de Micro e Nanotecnologias

Development of microfluidic tools for cancer single cell encapsulation and proliferation in microdroplets

Dissertação para Obtenção do Grau de Mestre em

Engenharia de Micro e Nanotecnologias

Orientador: Dr. Sara Abalde-Cela, Research Associate, INL

Co-orientador: Prof. Dr. Hugo Manuel Brito Águas, Associate Professor, FCT-UNL

Outubro, 2019

Júri:

Presidente: Doutor João Paulo Miranda Ribeiro Borges, Professor Associado com Agregação do Departamento de Ciência dos Materiais, da Faculdade de Ciências e Tecnologia da Universidade Nova de Lisboa;

Arguentes: Doutor Pedro Miguel Ribeiro Viana Baptista, Professor Catedrático do Departamento de Ciências da Vida, da Faculdade de Ciências e Tecnologia da Universidade Nova de Lisboa;

Vogais: Dr. Sara Abalde-Cela, Research Associate, INL;

FACULDADE DE CIÊNCIAS E TECNOLOGIA
UNIVERSIDADE NOVA DE LISBOA

Development of microfluidic tools for cancer single cell encapsulation and proliferation in microdroplets

Acknowledgments

Most of us are given clues to which roads we should take in life, whether they lead us somewhere promising or just as a form of natural progression. As I view it, I always searched of a way I could use my talents for the improvement of mankind, although becoming disillusioned most of the time. Out of nowhere, the field of nanotechnology became an area of interest, thanks to the noticeable achievement of many people working in the area. And now, even knowing some of those extraordinary people as my teachers, I cannot even fathom looking back at all the strides over these 5 years in obtaining my master's degree in Micro and Nanotechnologies.

First and foremost, I want to thank my mother, my father and my brother for always support me throughout all of my life, through all the achievements and hardships, even when things seemed the darkest, I could always find solace in them.

Also, I cannot forget all the friends I've made throughout my time in the university, helping each other through the hard times, and who I can still rely on.

However, the greatest endeavour I undertake was certainly during these last 9 months, trying to finish my thesis in the best way possible. All the people I've met during that made me stronger as a person, both mentally and emotionally and I must thank everyone for this experience. More importantly, I have to thank my supervisor, Dr. Sara Abalde-Cela, who not only guided me throughout all of my work, but also taught me all the tools I needed to master my talents, and who I look to as a source of utmost professionalism and dedication.

Also, I'd like to thank to some people who went out of their way to make my work more manageable. I would like to thank Alexandra Teixeira, who always provided a helping hand when possible, who showed me that we can do what the set our minds to if we learn to trust one another. Her commitment and enjoyment in this field are truly things I look in awe, and I hope that I can repay that kindness one day.

Most importantly, I must thank Kevin Oliveira, who became a sort of senior to me since he was taking his master's thesis ahead of me, and who I would always turn to when things didn't go according to plan. Since my work was largely inspired by the works he accomplished in his thesis, I can say that this thesis is a continuation of his labours as a master in Micro and Nanotechnology, and I hope all the best for his future as an engineer.

Also, I'd like to thank to Paulina Piairo and Cláudia Lopes for supporting me with the biological samples I needed to complete my work, but also for their friendship and words of encouragement, and Pedro Conceição, who always showed me how to keep cool when things just seemed too hard to take on.

Last but not least, I want to thank Prof. Hugo Águas for putting me in contact with International Iberian Nanotechnology Laboratory (INL), to Dr. Lorena Diéguez for assisting me with all the resources I needed to complete my work and for helping me for the first couple of months while I was adjusting, to my university (Universidade Nova de Lisboa) for allowing me to become a full-fledged master in Micro and Nanotechnology and to all my teachers who helped me along the way.

Abstract

The role of **microfluidics** in **liquid biopsy** as a more capable solution to address the monitoring of **cancer** progression in patients is gaining increasing attention. One out of the several difficulties in cancer monitoring resides with the offset between current cell growth techniques *in vitro* and the influence of the cellular microenvironment in proliferation. One application of **microfluidics** consists in the use of **microdroplets** to replicate the complex dynamic microenvironment that can accurately describe factual **3D models** of cancer cell growth. The goal of this thesis was to develop a set of **microfluidic-based** tools that would enable the encapsulation, proliferation and monitoring of single cancer cells in microdroplets. For this, a set of microfluidic devices made of **PDMS** for droplet generation and containment were developed by photo- and soft-lithography techniques, being tested and optimized to ensure single cancer cell encapsulation. After the optimization of the droplet generation parameters in terms of droplet size and long-term stability on-chip, the best performance conditions were selected for cell growth experiments. Different densities of **MDA-MB-435S** cancer cells were combined with various percentages of **Matrigel®**, an extracellular matrix supplement, to promote cell proliferation. As a result, it was possible to monitor droplets with cancer cells for a range of 1-20 days. A preliminary observation showed signs of cell aggregation, indicating that the tools developed during the thesis have the potential of developing **3D cancer spheroids** from **cancer single cells**.

Keywords: Microfluidics, liquid biopsy, cancer, microdroplets, PDMS, 3D spheroids, cancer single cells.

Resumo

O papel da **microfluidica** no campo da **biopsia líquida** começa a ganhar cada vez mais atenção ao revelar-se como uma solução mais capaz na monitorização da progressão de **cancro** em doentes on- cológicos. O foco das dificuldades mais prementes na monitorização da doença encontra-se na desfa- sagem entre os métodos convencionais de crescimento celular *in vitro* e a representação actual da influência de microambientes celulares como um modelo 3D. Uma das áreas de especialidade do ramo da **microfluidica** consiste no uso de **microdroplets** como um meio de recriação de ambientes com- plexos que possam replicar os modelos actuais de crescimento celular em 3D. O objectivo principal desta tese consistiu em desenvolver estruturas de **microfluidica** que permitissem o encapsulamento, a proliferação e a monitorização de **células cancerígenas individuais** em **microdroplets**. Para tal, um conjunto de dispositivos de microfluidica à base de **PDMS** para formação e contenção de microdro- plets foram desenvolvidos recorrendo a técnicas de *photolithography* e *softlithography*, sendo posteri- ormente testados e optimizados para garantir o encapsulamento de **células cancerígenas individu- ais.** Depois da optimização dos parâmetros de formação de microdroplets relativos a tamanhos obtidos e estabilidade a longo prazo, o conjunto dos melhores parâmetros foi selecionado para experiências de crescimento celular. Diferentes densidades celulares de células **MDA-MB-435S** foram combinadas com diferentes percentagens de **Matrigel®** para acelerar o crescimento celular. Dentro dos resultados obti- dos na tese, foi possível monitorizar microdroplets até 20 dias após a sua formação e também se veri- ficaram sinais de agregação de células em microdroplets, reforçando o potencial destas técnicas em formar estruturas **esferoides 3D** a partir de células individuais.

Palavras-chave: Microfluidica, biopsia líquida, cancro, microdroplets, células cancerígenas individuais, PDMS, esferoides 3D,

Table of Contents

List of Figures

List of Tables

List of Abbreviations and Acronyms

CSCs – Cancer Stem Cells

CCL – Cell Culture Lab

CTCs – Circulating Tumour Cells

DWL – Direct Writing Laser

DMEM – Dulbecco's Modified Eagle's Serum

EMT – Epithelial-Mesenchymal Transition

FBS – Fetal Bovine Serum

Gen. - Generation

HTS – High-throughput screening

IPA – Isopropyl Alcohol

LDPE - Low-density polyethylene

PS-1 – Pico-Surf™ 1

PDMS - Polydimethylsiloxane

PGMEA – Propylene Glycol Monomethyl Ether Acetate

SD – Standard Deviation

List of Symbols

$Q_{cont.}$ – Continuous phase flow rate

$Q_{disp.}$ – Dispersive phase flow rate

Q_{oil} – Flow rate of oil

Q_{cells} – Flow rate of cells

P – Poisson distribution

k – Number of cells in a microdroplet

λ – Average number of cells per microdroplet volume

ϕs – Cell density per volume of solution

ϕd – Number of microdroplets generated with given volume of a dsolution

r - Radius of microdroplets obtained

Motivation and Objectives

Cancer continues to be a leading cause of death worldwide, being second only after cardiovascular diseases[1]. In 2018, about 9.6 million deaths and 18.1 million new cases were recorded[2–4], and according to some reports, by 2020, it could become the main cause of death worldwide[5]. Those statistics can be attributed to a rapidly increasing aging population and added risks attributed to socioeconomical development[6]. Treating patients with cancer becomes an unfathomable challenge in large part due to two major factors: model prediction of spread after the primary tumour starts extruding cells to further organs (metastasis)[7,8] and increased economic burden on the most advanced stages of cancer treatment[9–11]. At least 90 % of all cancer deaths are attributed to the occurrence of metastasis. One on the main pathways by which tumours can expand to distant organs relates to the dissemination of circulating tumour cells (CTCs), which are produced from a mature tumour and enter the bloodstream, presumably by means of the endothelial-mesenchymal transition (EMT), progressing into distant tissues and organs, and eventually causing metastasis.

Nowadays, the study of single cells is revolutionising the way we approach and understand cancer supported by the use of **technology for biology**[12]**.** By using **single-cell omics (**genomics, transcriptomics and/or metabolomics) it is possible to obtain information at the single-cell level and not only averaged data across a bulk population of cells, as in the past. However, it is also important to be able to relate the information we obtain from each single cell of interest to its proliferation mechanisms, growth dynamics, metabolism and clonal evolution. A continued unsolved challenge is the high-throughput and controlled generation of cancer models deriving from a single-cell. In this sense, **spheroids,** sphere-shaped aggregates of cells can be used as **3D cancer models**, having been reported to accurately mimic the characteristics of *in vivo* solid tumours with potential for therapeutic screening and drug testing[13],

As per bottlenecks and challenges described above, the main goal of this thesis was to explore the possibility of the use of microdroplets technology for the encapsulation of cancer single cells for their continuous monitoring while proliferation into 3D spheroids. For this, several specific objectives were defined as follows:

1. Fabrication of a set of microfluidic and microdroplets devices for the encapsulation of single cancer cells.
2. Interfacing the microdroplet generation with reservoirs for the incubation of encapsulated cell in microfluidic devices.
3. Optimization of the microfluidic conditions that may result in a robust platform for the single-cell derived 3D spheroids proliferation and monitoring.
4. Pre-testing the developed platforms with cancer cells from lab-grown cancer cell lines.

1 Introduction

1.1 The disease known as Cancer

Cancer derives from damaged somatic cells in the body[14–16] after an accumulation of mutations that can be derived from routine processes for example, DNA repair, transcription and replication[17–19]. Those mutations can also be caused by multiple punctual modifications to chromosomal structures or enzymes, epigenetic alterations[20] or caused by exogenous infections, for example oncoviruses[21,22]. Cancerous cells can start from any point in the body, from specific cells in organs like the heart and kidneys, to the bone marrow[23–25]. Cells in the body engage in the process of division and multiplication, which can include several steps. During any of these steps, erroneous mismatches can appear, which can sum up to an even greater alteration of the original genotype[26–31]. The normal path of progression of cancer starts when a cell develops an erroneous version of its original genome and starts to produce abnormal copies of itself, up to the point where entire tissues are affected[7]. The worst outcome of the disease is the onset of metastasis, where an uncontrolled spread of damaged cells, so-called circulating tumour cells (CTCs), spread throughout the body, making use of the circulatory and lymphatic systems to travel throughout the body[32–34], and seeding secondary tumours in different tissues and organs. When the damaged cells start replacing the functional cells in the organs, those organs stop functioning properly, eventually leading to death due to multiple organ failure[20]. About 90% of all cancer related deaths are attributed to the occurrence of metastasis[35].

One of the major challenges in cancer is that it is a highly heterogeneous disease at many different levels: intra-tumour, inter-tumour and also amongst different patients. The heterogeneity in cancer has been defined as one of the hallmarks in cancer[8,23,36–42], as well as in metastasis, limiting the accurate diagnosis that may enable the identification of the appropriate druggable mutations, eventually resulting in poor efficacy of most treatments[37,43,44].
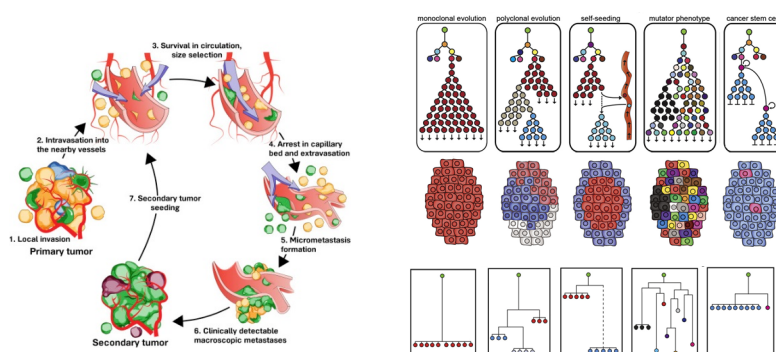
Figure 1 – Composite figure depicting the process of tumour propagation (A) and the different forms how heterogeneity can be expressed by multiple phylogenetic trees (B) (Pictures taken from references [34,47]).

1.2 Circulating Tumour Cells (CTCs) and Liquid Biopsy

According to several reports, CTCs would have the ability to induce metastasis into distant organs, but only in a fractional number of the total produced by the tumour. Discovered in 1869 by Thomas Ashworth[45], their role in cancer development only came later, when several other studies managed to demonstrate the correlation between the number of CTCs present in the bloodstream and the risk of a patient developing metastasis[46–52]. Also, CTC numbers can serve as an estimator of overall rate of survival for patients and therapy efficiency. So, a possible logical route in order to augment efficiency in the treatment of cancer would be for the detection and analysis of those CTCs. The technique of liquid biopsy in particular permits to extract CTCs from a patient's blood in a facilitated way and without causing too much trauma to their patients[53,54]. Unfortunately, CTCs have a low time window of survival, with only 0.1 % of CTC being able to survive and only 0.01 % being viable enough to induce metastasis, being classified as exceedingly rare cells[47,50,55–57].
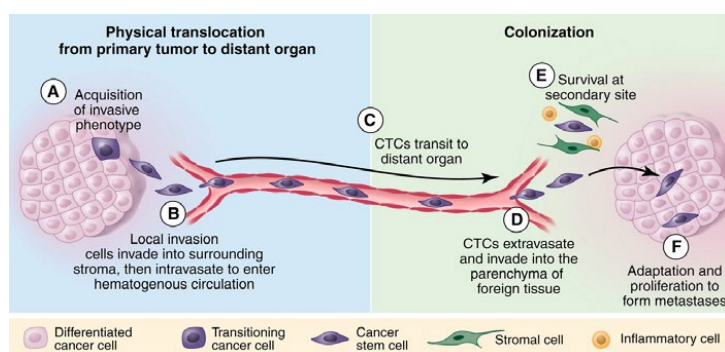
Figure 2 – Schematic figure that shows how CTCs travel through the body to propagate into distant organs (Ref. from article[58]).

In order to tackle the difficulty in extracting CTCs from whole blood samples for their isolation[58], characterisation and analysis, several technologies were developed, involving different techniques such as immunomagnetic separation, microfluidic sorting[53], gradient centrifugation[59] and dielectrophoresis separation[50,60–67].

The process of metastasis is endowed with significant advantages that allow it to become chaotically efficient in confusing the immune system and rendering medical treatments ineffective[8,20,42,68]. For example, enhanced motility and permeation into tissues[33], stress-induced plasticity to overcome constrains in growth, capability in modulating local microenvironments into more propitious ones for tumour cells and the ability to disseminate into distant organs through CTCs[48,55]. As such, there is still a remarkable gap on understanding the functionality of those isolated CTCs, which are a snapshot of the current state of the disease.

1.3 Spheroids and 3D Cancer Models

Based on past research, researchers became aware of the potential that 3D spheroids, sphere-shaped aggregates of cells, hold as a model for emulating how cancer cells form complex structures like those

found in cancer patients behave[69–74]. Spheroids can reproduce several features identical to those found in tumours, for example, oxygen and nutrient depletion, culture heterogeneity[75] and proliferation rates. Spheroids are also of interest to understand the efficacy of therapies, since they can emulate the different ways cancer cells resist to different drugs and irradiation treatments[72] for example, by inducing DNA double-strand breaks that can result in further mutations that can make the cells even more resilient, generating chemotherapy-resistant cancer stem cells (CSCs) that can help in maintaining the tumours viable and by making their microenvironments less effective for drugs by altering their pH levels to become more acidic[76]. They can also potentially generate CTCs of their own[57,62]l, making spheroids an acceptable model to predict cancer mechanisms of propagation.

However, in the issue of generating spheroid models from single-cell populations, there are two bottleneck situations that further complicate things when attempting to postulate a cancer model for CTCs:

1. The current methods for cell growth heavily rely on 2D-based techniques, for example, hanging drop[67,77], non-adhesive surfaces[78], suspension in microwell plates[67,79]. They reportedly fail to emulate the complexities involving the microenvironment in which tumours grow, in specific, the effect of the extracellular matrix in growth[75,80–84], the lack of spatial constrictions[85], the metabolic requirements to sustain cancer cells for specific long periods of time (temperature, pH, CO_2 levels)[86] and the influence of the immune system in forcing the cells to stablish preferential populations by natural selection[72]. Table 1 enumerates the numerous ways in which 2D and 3D cell cultures differ from each other.

2. CTCs have a very low rate of survival in the bloodstream, a lower rate of ability to induce metastasis and even lower rate of isolation from liquid biopsy samples[35], so, it becomes extremely difficult to obtain enough viable samples for *in vitro* experiments and *in vivo* xenografts[63,87].

Table 1 – Table enumerating the differences between 2D and 3D cell cultures[88].

Characteristics	2D cell culture	3D cell culture
Morphology	Cells grow over a flat surface	Formation of spheroids
Cell-cell interaction	Limited cell contact, only on edges	Interactions similar to in vivo conditions
Medium distribution	Medium is distributed evenly, not like in vivo	Medium gets scarce closer to the core of the culture, generating an hypoxic core
Expression	Differ significantly among cells	Models more approximate to reality
Differentiation	Moderate differentiation	Noticeable differentiation
Viability	Sensible to cytotoxin	More resistant to external factors and more viable
Drug sensitivity	More responsive to drugs (less accurate)	Less responsive to drugs (more accurate)
Sub-culture time	Up to 1 week	Nearly 4 weeks

Taking both problems in consideration, the best way to study the matter of how single CTCs can initiate the metastatic process is to conceive a method of proliferating single cells in 3D-like structures. The spheroid structure previously mentioned as a good model for a 3D cell structure can replicate *in vivo* conditions of solid tumours with potential applications for therapeutic purposes[42,76]. But the production

of spheroids can be an arduous process, with a lot of variability between spheroid size and phenotypical profile[73] and can also be difficult to analyse morphology and viability of samples without high-resolution technology, like confocal microscopy. A good way to predict cancer growth is to project experiments that can obtain high-throughput screening (HTS) results from replications of the same experimental conditions[74,89]. But designing multiple experiments for complex structures like tumours can be too costly and may not consider the individual nature of cancer cells in driving the metastatic process, from metabolism requirements, to clonal formation and to proliferation speed. To that end, microfluidic techniques may provide a solution for the low-throughput difficulties associated with spheroid growth and proliferation[74].
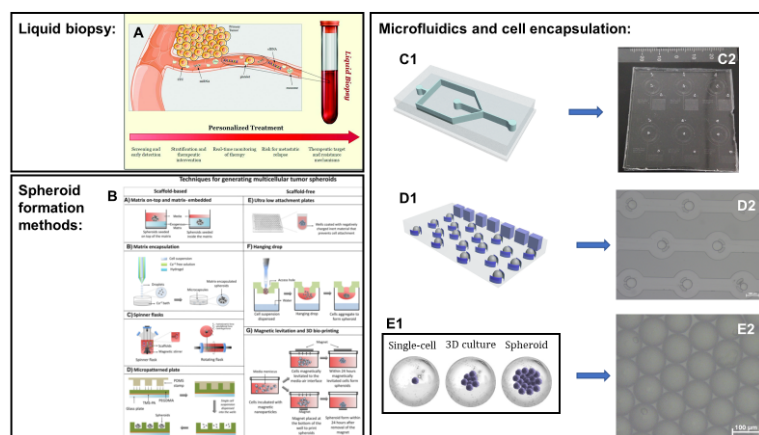
Figure 3 – Descriptive figure with all of the different elements that shape the premise of the thesis, with an image depicting liquid biopsy characteristics[65] (A) different spheroid formation techniques[86] (B) and the different steps regarding microdroplet generation, retention and observation of cancer spheroid formation from illustrative images (C1, D1, E1) to real time images (C2, D2, E2).

1.4 Microfluidics, Microdroplets and Cell Encapsulation

The first notions about microfluidics came in 1965 by Richard Sweet, upon the discovery of inkjet printing techniques. In 1979, Terry et al. demonstrated the potential in microfluidics to produce devices that could manipulate fluids on the micro-scale, and in the 90s, several articles revealed the potential in microfluidics to handle biological applications[90], especially regarding the use of polydimethylsiloxane (PDMS) as a material for biological analysis due to its biocompatibility and easy production[67,91].

The control of very small volumes of liquids within microscopic-sized channels, combined with fast producing techniques of an affordable nature and the ability to time reactions down to the microsecond or up to sets of hours[92–94] made the field of microfluidics very valued in industry applications and biology research[71,95,96]. By the start of the 21st century, microfluidics had branched off into several different specialties within the field, like digital microfluidics, organ-on-a-chip devices[97,98], paper-based devices[67,99] and droplet microfluidics[42,74,96,100–102]. The last subgenre mentioned, also known as segmented flow microfluidics or microdroplets technology, will be the starting point for the project of this thesis.

Microdroplet generation is based on the principle of how emulsions are formed[102,103]. When two immiscible fluids with different viscosities meet one another (entering into a laminar flow regime)[94], the two fluids avoid interacting with each other directly[104]. By controlling the point of contact of both liquids, it is possible to generate droplets[105]. The typical geometry for the formation of droplets revolves around the

flow-focusing geometry microfluidic devices[102,105–109], in which the two liquid phases enter through two different openings of the channels defined as inlets[67,110]. One of the inlets is for the dispersive phase (phase that will get encapsulated into droplets) and the other inlet is for the continuous phase (phase in which the droplets will travel and be contained)[111]. The two phases encounter each other at a T-shaped junction and form droplets upon contact through a "cut" motion[104,107,112,113]. The droplets then follow the flow through a third channel defined as an outlet and exit the microfluidic device[67]. By controlling the flow rate of both liquids and the width of the intersection[96,102,109,114], microdroplets can be generated at a specific frequency with well-defined sizes at high monodispersity[93,104,106,115,116].

Generated droplets are the perfect isolated environment that allow to control chemical reactions and to separate multiple components. A certain number of studies have already dwelled in the encapsulation of different types of cells[74,117], from bacteria[118] to mammalian cells[119]. The focus on those studies has been mostly in distinguishing samples within droplets to produce high-throughput results[101,120], but not many endeavoured in maintaining their cultures for prolonged periods of time. Surpassing the limitations that reside in microdroplet encapsulation would allow to produce a promising tool for cell analysis in long-term studies[59,93].

With the situation fully described and taking into account the challenges to overcome in generating CTC spheroids based on single-cell derivation models[66], the objective of this thesis is to perform a proof-of-concept high-throughput microdroplet production method for the encapsulation of single cancer single -cells and promote the formation of 3D-spheroids. The latter can be only realised after testing different parameters such as flow rates for continuous and dispersive phase, type of moulds for droplet generation and contention, type of cancer cells to encapsulate, addition of extracellular matrix-simulating products, incubation and monitoring settings. In theory, the idea of encapsulating cancer cells in microdroplets could provide a facilitated and affordable method to isolate cancer cells and monitor their progression using a microscope, as well as increasing the high-throughput fabrication of 3D spheroids. As mentioned before, microdroplet techniques are known for providing high-throughput results, allowing for a statistical observation of predominant phenotypes from samples of patients. With such results it would be possible to adjust treatments with a higher rate of success, besides providing new insights on the understanding on single-cell replication mechanisms and cell malignancy and colonisation potential.
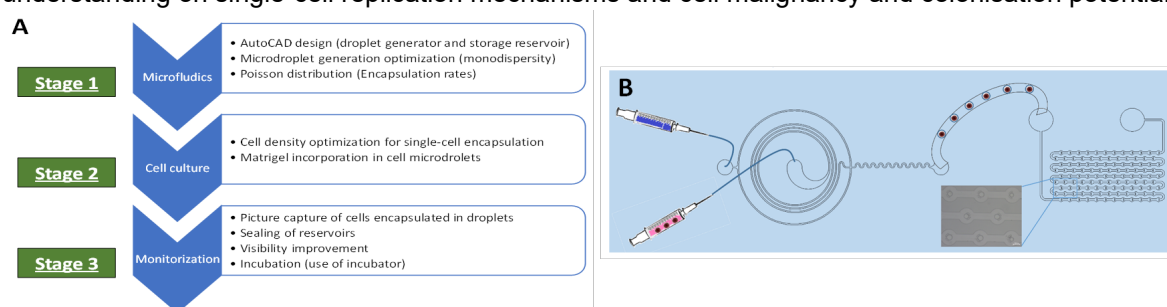
Figure 4 - Descriptive figure of the layout planned for the duration of the thesis (A) and an illustrative figure which shows the end result of all the stages of the thesis coming together into conceiving a method for cell encapsulation and monitoring (B).

2 Materials and Methods

Materials: All the chemical haven been purchased from Sigma-Aldrich unless otherwise stated.

2.1 Fabrication of the PDMS devices used for cell encapsulation and growth monitoring

For the assembly of the polydimethylsiloxane (PDMS) devices, two specific microfabrication techniques were utilized: photolithography and soft lithography[121]. The application of those techniques is summarized in the following sections.

2.1.1 Fabrication of the master SU-8 mould on silicon wafer

The use of the photolithography technique was for the purpose of creating a master SU-8 mould that will serve to imprint the microfluidic channels of the PDMS devices, upon the use of soft-lithography for replication.

All processes regarding the fabrication of the SU-8 mould were executed within a class 100 (according to the FED STD 209E, in ISO 14644-1 standards is the ISO 5) micro and nanofabrication cleanroom of around 700 m^2 effective space.

The first step for the fabrication of the SU-8 mask started with the design of the microfluidic channels on a writing program. The software Autodesk® AutoCAD 2019 was utilized to draw the design outlines to be replicated on the master, with the completed drawings exhibited on Annex 1. The AutoCAD file was processed for the direct writing laser (DWL) machine [DWL 200, Heidelberg Instruments]. The pattern of the complete design was inscribed on an acrylic hard mask that would confine the passage of UV-light during the exposure step of the photolithography process. The SU-8 master mould was deposited on top of an 8'' (20.32 cm) silicon wafer by spin-coating. Approximately 5 mL of SU-8 were poured on the centre of the wafer, with the wafer held in the centre of the spin-coater machine. The protocol followed for the spin-coating was a 3-step process, starting with 500 rpm for 10 s with a ramp of 5 rpm, followed by 1000 rpm for 32 s with a ramp of 1.7 rpm and finishing with 100 rpm for 1 s with a ramp of 2 rpm, in order to obtain an estimated layer thickness of 80 μm. The wafer was then subjected to a soft-baking process with 2 different temperatures, using 2 different hot plates. The wafer was placed over the first hot plate at 65 °C for 3 min, and then it was moved to the other hot place at 95 °C for 9 min, and then removed in order to cool down before UV-light exposure. Using the hard mask fabricated beforehand and properly placed in the holder between the light source and the wafer, the wafer was irradiated with a 375 mJ cm^{-2} dose of UV-light for 10.9 s. The exposed wafer was subjected to a post-exposure 3-step process. The wafer was placed over the first hot plate at 65 °C for 2 min, moved onto

the second hot plate at 95 °C for 7 min and placed back to the first hot plate for 2 more min, to generate a ramp for the cooldown process. The wafer was then developed, using propylene glycol methyl ether acetate (PGMEA) as the developer and isopropyl alcohol (IPA) to wash off the developer from the wafer. The development process lasted for 7 min, by submerging the wafer on a glass tub slightly filled with the developer while gently stirring it, and after passing the wafer to another glass tub filled with IPA to remove the developer from the surface.

Once the features of the design were clearly visible over the mould, the wafer was then placed in an acrylic container and taken to the profilometer (KLA Tencor P-16+ Surface Profiler), to obtain the real values of the SU-8 thickness throughout the surface of the wafer. The values were stored in a datasheet and the wafer was taken to the microfluidics lab for the soft-lithography process.

2.1.2 Fabrication of the PDMS devices by soft-lithography

The soft-lithography process consisted of a pouring-solidify-peeling sequence. First, a PDMS solution of about 100 g in total was prepared using a combination of elastomer and curing agent in a 10:1 ratio [SYLGARD™ 184 Silicone Elastomer Base + Curing Agent (The Dow Corning Company] and then poured over the master mould. "Blank" PDMS moulds were prepared by pouring the remnants of the solution over empty Petri dishes (previously cleaned by N_2). The filled master and Petri dishes with "blank" PDMS were de-gassed on the degasser [Bel-Art Products] by a primary vacuum pump [Agilent Technologies, IDP-3 Dry Scroll Vacuum Pump] until no air bubbles could be seen on the surface. Following, they were put in the oven [Heratherm Oven, Thermo Scientific] for a minimum of 1 h at 65 °C, until they were completely solid. The solidified PDMS mould over the wafer was removed using a scalpel and slowly peeled off by hand motion. With the moulds replicated on the PDMS, a biopsy puncher with 1 mm diameter for the punch (Kai Medical) was used to open holes in the inlet/outlet zones and the replicated PDMS was bounded to the "blank" PDMS through surface activation by resorting to an oxygen plasma chamber Plasma Cleaner (PDC-002-CE, Harrick Plasma) with UV-light irradiation. The completed device with the sealed microfluidic channels was functionalized by injecting Aquapel® into the channels with the aid of a 1 mL syringe, a syringe needle (0.76 mm ID, INSTECH) and a piece of low-density polyethylene (LDPE) Portex™ (Smiths Medical) tubing, following by the injection of 3M™ Novec™ HFE-7500 oil (molecular weight - 414 g mol^{-1}; viscosity – 0.77 cSt; liquid density – 1614 kg m^{-3}) to remove the Aquapel® from the channels before crystallization could occur.

2.2 Microdroplet formation

2.2.1 Cell culture preparation (seeding, proliferation, removal)

For the growth of cancer cell cultures, a batch of MDA-MB-435 (MDA) cancer cells (ATCC, HTB-129) was cultured in Dulbecco's modified Eagle's medium (DMEM; Gibco), supplemented with 10 % of fetal

bovine serum (FBS, Gibco) to provide growth factors and a dose of penicillin/streptomycin (Corning) to prevent contamination in 1 % of the total volume. The complete solution was incubated at 37 °C, with CO_2 levels at 5 % of the complete composition of the enclosed air.

To obtain a vial of MDA cells ready for encapsulation, several steps were executed for that purpose. First, MDA cells were placed in 5 mL of medium, inside a T25 (25 cm^2 surface area) flask, then the T25 flask was left alone in the incubator until the vial could be considered confluent under optical microscope visualization (about 90 % of the total seeding surface covered). The next step was trypsinisation, starting with the removal of the starting medium (due to by-product accumulation) and then followed with the addition of 0.5 mL of Trypsin for 5 min and placing the flask in the incubator at 37 °C, 20 % of O_2 and 5 % of CO_2 to detach the cells from the seeding surface. The process was followed by the addition of 4.5 mL of the medium described initially, in order to nullify the effects of Trypsin (BioConcept, 100 mL). With the cells in a suspended state, the following step was to estimate the number of cells present in the solution. For this, about 10 μL of the MDA cell solution was added, along with 10 μL of Trypan Blue Solution (Corning, 100 mL). A haemocytometer (Figure 28, Annex 3) was utilized to count the viable cells placed on each of the 4 quadrants of its surface.

The calculations for the estimated number of cells per mL were performed using the following formula:

$$\frac{counted\ cells}{number\ of\ quandrants\ counted} \times dillution\ factor\ \times 10^4$$

However, since the density desired is in the order of millions, it is necessary to convert from 10^4 to 10^6. Once the final value is obtained for 10^6 cells per mL, adjustments were made to get the correct value for cell density that is necessary for the experiments, extracting as much is necessary from the MDA cell solution into a 1.5 mL Eppendorf.

2.2.2 Encapsulation process

The encapsulation process was initiated by the selection of the PDMS moulds made previously for microdroplet encapsulation. The continuous and dispersive phases were selected, with the solution of cells prepared as described in chapter 2.2.1 and added Matrigel®[122] as the dispersive phase (Q_{cells}), and a solution of FC-40 + Pico-Surf™ 1 (PS-1, Sphere Fluidics, Ltd.) in 2 % of the total volume as the continuous phase (Q_{oil}). The solutions were then placed inside 1 mL syringes attached to syringe needles (0.5 mm inner diameter), with the needle tips connected to a portion of LDPE tubing (0.38 mm inner diameter). The syringes were then placed on two separate syringe pumps (New Era Pump Systems) and the extensions of the LDPE tubing of the syringes were connected to the two inlets for the continuous and dispersive phases. The outlet of the mould responsible for droplet formation was connected to the inlet of the mould with the reservoir design for droplet capture by a portion of LDPE tubing and the outlet of the mould with the reservoir design was connected to a small plastic Eppendorf of 1 mL. The syringe

pumps were programmed for each of the syringes, with defined flow rates of 500 µL hr^{-1} for the continuous phase, 100 µL hr^{-1} for the dispersive phase and with both pumps assuming a hydrodynamic radius of 4.7 mm. The reasoning for the values of both flow rates was stablished in order to obtain a ratio between the continuous and dispersive phases (Q_{oil}/Q_{cells}) of 5. The observation of droplet formation was done under an inverted optical microscope (Microfluidics Microscope Nikon ECLIPSE MA200) with a 5× objective, with saturation and brightness settings on the maximum level. In order to seal the reservoirs, a pair of metal tips was heated with a lighter and put in contact with the portions of LDPE connected to the inlet and outlet, to shut them tight by contracting the channels through heat, without completely melting them. For the purpose of preserving the reservoirs for several days, an additional process was performed, which consisted of placing the reservoirs in a Petri dish, fixating them to the surface with glue tape, filling it with Milli-Q (MQ) water until it nearly reaches the top surface of the reservoirs and closing the Petri dish with its complimentary lid.

2.2.3 Calibration of average droplet size and optimization of cell encapsulation rates

After successfully sealing the reservoirs, pictures from the interior of the reservoir were taken, using the NIS-Elements F 3.2 software. For picture capture specifications, the images taken were in bright field conditions (unless when alterations were made) and saved in .tiff format. Afterwards, the images were processed in ImageJ to analyse the average droplet diameter obtained, and the encapsulation rates of cancer cells captured in microdroplets. For the average droplet diameter measurements, Milli-Q water was used as the dispersive phase, and for the calculation of the number of cells encapsulated per droplet, a solution of MDA-MB-435 and DMEM was used as the dispersive phase. These experiments were performed in order to discover the optimal values for the ratio between flow rates of the continuous and dispersive phases (Q_{oil}/Q_{cells}) that could allow for a balance between a majority of single cell encapsulation and capture of samples with more than 100 droplets per picture.

2.3 Cell encapsulation

2.3.1 Experiment outline (solutions and moulds used)

In preparation for the experiments regarding cell encapsulation and monitoring of growth, several moulds were tested, for both droplet generation and storage. The main mould type decided for droplet generation was the circular Dean flow mould with a T-section length of channel entry of 80 µm. For droplet conservation and long-term observation, the linear reservoir was chosen. For the first set of experiments, four different solutions were prepared for the experiments to serve as dispersive phase solutions. The composition of solutions for continuous and dispersive phase are as described previously

in chapter 2.2.1 for the dispersive phase, with 4 different percentages of Matrigel® added for each solution based on total volume (1 %, 2 %, 4 %, 8 %) and in chapter 2.2.2 for the continuous phase, with the flow rates for each solution described in chapter 2.2.2. The cell density for all 4 dispersive phase solutions was approximately 2×10^6 cells mL^{-1}. A schematic of the complete representation of the experiments is represented in Figure 5
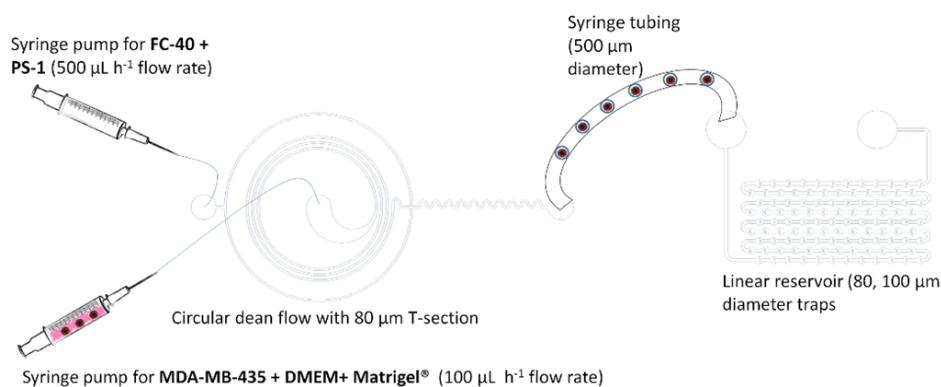
Figure 5 – Representative layout of the encapsulation process of MDA-MB435 cells using a microdroplet generator (circular dean flow) and retention process within the microdroplet reservoir (linear reservoir).

2.3.2 Preparation of the sealed reservoirs for incubation

After sealing the reservoirs using the method as described in Chapter 2.2.2, the reservoirs were carefully placed in a clear plastic box, restrained inside using glue tape, and afterwards, the box was filled with Milli-Q water, up until the level of the water nearly reached the top surface of the reservoir. The purpose of this procedure is to prevent the diffusion of water and oil through the PDMS, helping to maintain the contents of the reservoir stable. A live picture of the preparation process can be seen in Figure 27, Annex 3.

After the reservoirs were properly closed in the plastic box, the box is transported to the cell culture lab (CCL), doused with ethanol 70 % to sterilize it and then placed in the incubator, which was assumedly normally programmed under the following conditions: 37 °C, 20 % O_2 and 5 % CO_2.

3 Results and Discussion

This chapter focuses on the overall results regarding every step of the master thesis' work, from mould design to cell encapsulation in microdroplets. Each part of the project encompasses a detailed analysis of the aspects that constitute it. The results obtained have been separated into different characteristics that can be extrapolated to classify the outcome of the experiment. A schematic of this thought-process is represented in Figure 6.
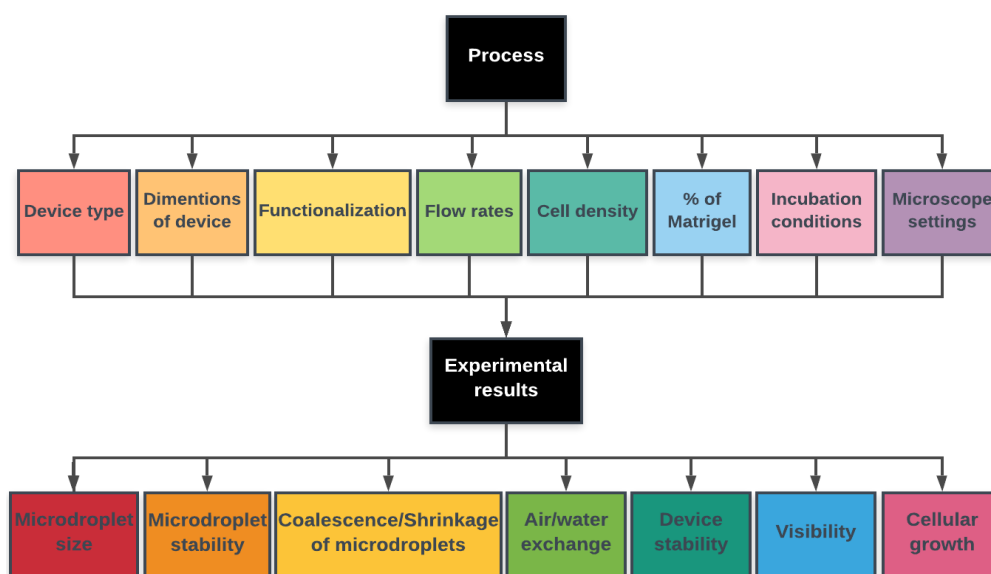
Figure 6 - Representative schematic of the aspects analysed throughout the thesis (before and after the experiments were performed).

3.1 Master mould optimization

The fabrication of the master mould was done resorting to previously performed techniques of photolithography done in the clean room. The expected results were based on previous experiments, averaging certain values after several fabrications were done. The protocol described in chapter 2.1.1 of Materials and Methods was conceived to obtain an expected channel height of 80 µm, even with slight variations of exposure or development time. The results of the profilometer revealed a significant reduction of the height of the channels, ranging from 49.43 to 56.13 µm, which for the sake of simplicity it will be considered as an average of 52.5 µm of photoresist thickness across the wafer. (Figure 31, Annex 4). Figure 7 illustrates the complete layout of the design (Figure 7A), and the three different types of designs developed and fabricated. (Figures 7B, 7C and 7D).

Figure 7 - Composite figure with all of the designs developed during the thesis: (A) – Layout of the devices for the hard mask fabrication; (B) – Dean flow microdroplet generator with amplification of the t-section with 120 μm width between all channels connecting to the cross-section; (C) – Composite mould with 80 μm trap size and T-section width; (D) – Linear reservoir with 100 μm width traps, 12 traps per each of the 17 lines.

As to the matter of the loss of thickness of the SU-8 photoresist over the mask, the possible causes for this may reside with either a soft baking executed too irregularly or an overdeveloped mask from staying too long in contact with the PGMEA developer[123]. At a second due over of the master (due to the first one having been broken), several issues were revealed regarding the adherence of the SU-8 2025 photoresist to the wafer, which may indicate that there might be issues with the current batch of SU-8, might have affected the overall stability of the master. It might be required to analyse and possibly replace the current batch of SU-8 to prevent similar issues.

3.2 Device functionality

As part of the workplan of the thesis, the design and fabrication of a set of moulds was conducted. The moulds conceived this thesis were inspired in the designs of the Generation (Gen.) 2 devices (Annex 2) designed in previous works. Three types of devices were conceived addressing the following aspects:

- **Circular Dean flow microdroplet generator** (Figure 7B): Based on the previous design of the Dean flow microdroplet generator used in the Gen. 2 Dean flow devices (Figure 23-A1, Annex 2), the central spiral architecture to induce Dean flow to space out cancer cells was repurposed, modifying the remaining channels to remove the existence of 90° corners that could compromise the functionality of the device if something were to block those passages and also by increasing the widths of the channels from 80 μm to 120 μm to alleviate the increased pressure of liquids when passing through the spiral channels, which could compromise the bonding process of the PDMS to the substrate when the flow rates were increased to higher levels[112,114];

- **Linear reservoir** (Figure 7D): This design was repurposed almost entirely from the original design of the Gen. 2 linear reservoirs (Figure 26, Annex 2), only making the channels with 120 μm of width and increasing the number of traps per line and the number of straight lines;

- **Combined device** (Circular Dean flow + linear reservoir, figure 7C): This device was conceived to address the problem with sealing procedures being imperfect at times and also to see if the coalescence of microdroplets occurred during the passage from the microdroplet generator to the reservoir via LDPE tubing;

In order to explore the effect of different sizes of microdroplets in the encapsulation rates of cancer cells, the three types of devices were fabricated in 3 different sizes: 80 µm, 100 µm and 120 µm, whether for the width of the channels which form the T-section of the circular Dean flow devices or for the width of the traps within the linear reservoirs. (Figures 21 and 22 in Annex 1) However, the fabrication of the master was only performed at a later stage of the thesis, so for the time being, some of the results were obtained by resorting to the previous masters already fabricated in the cleanroom for use in previous works (Figures 23-A1 and 23-B1 in Annex 2). The three types of moulds were tested regarding their design specifications and how their results hold up when compared to previous versions of designs. The microdroplet generator moulds were tested in their capacity to produce samples of monodispersed microdroplets, the linear reservoirs were tested in their capacity to entrap and retain droplets in the designated trap locations and the combined mould was only tested as to the practicality of joining the microdroplet generator and a reservoir together in the same mould.

3.2.1 Microdroplet size optimization

As discussed in several articles, there are several factors which influence the size of microdroplets being directly connected to the ratio between the flow rates of the continuous and the dispersive phases, but in particular with the flow rate of the continuous phase, which is the one that "slices" through the dispersive phase[106]. But other factors which play a significant role in microdroplet production are the geometry of the device, the viscosity of the continuous phase and the velocity with which the two phases travel the channels[102,108,109,111]. Since testing all those parameters would be a time-consuming effort, it was decided that the focus of the thesis would be in adjusting the dimensions of the new devices with the flow rates of the continuous and the dispersive phases. To that end, several calibration experiments were performed to fine-tune the microfluidic devices as to the range of sizes that the produced microdroplets could obtain.

The circular dean flow microdroplet generators were tested in their capacity to produce monodispersed microdroplets in samples of at least 100 microdroplets per picture frame. In order to measure monodispersity obtained from microdroplet generators, pictures of collected samples were taken, deconstructed and analysed. To that end, it is important to explain in detail how microdroplets were analysed in terms of monodispersity by size, starting with the process of sealing microdroplets inside the reservoir. First, the microdroplet generator was put into a functional state, by adjusting the flow rates of the continuous and dispersive phases from the syringe pumps' control panel. Second, a portion of LDPE tubing was cut and connected to the outlet termination, leaving the unconnected end of the tubing free. Third, a few minutes were spent waiting for the microdroplets to stabilize as they travel through the severed LDPE tubing, followed by extracting a sample of the contents within the tubing and placing it over a glass lens to observe if the microdroplets appeared monodispersed under the microscope. Once monodispersity was confirmed, the unconnected end of the tubing was placed in the inlet of the reservoir. Fourth, while

observing the microdroplets entering the reservoir continuously and after a significant number of micro-droplets were located inside the reservoir, the ends of the LDPE tubing connected to the inlet and outlet of the reservoir were sealed using the method referred in chapter 2.2.2 of the materials and methods section (burning tips). Once the reservoir is properly sealed, pictures of microdroplets within the reservoir were taken in a matter that at least 100 microdroplets could fit within a picture capture. Fifth, using the ImageJ program, the images were processed in a way that outlines the microdroplet surface form the rest of the background, using a bandpass filter and then adjusting the threshold until the circular shape of the microdroplets was properly accentuated in the resulting picture. To complete the monodis-persity analysis, the surface area of the microdroplets was measured and registered in an Excel spread-sheet. A descriptive figure illustrating the entire process can be seen in Figure 8.
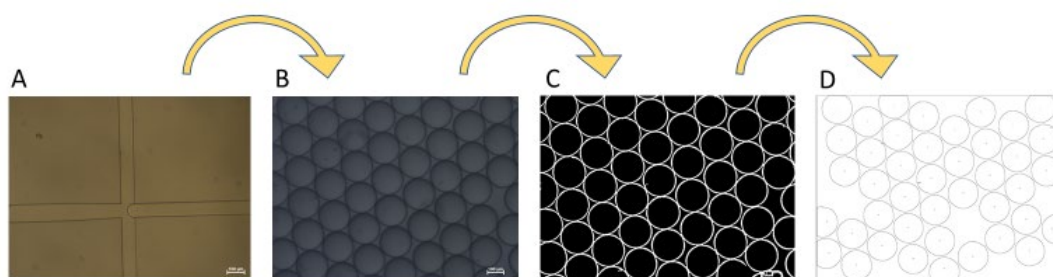
Figure 8 - Illustrative figure of the process regarding analysis of microdroplet monodispersity of the samples. A) Observation of microdroplet formation under optical microscopy; B) Picture capture of the microdroplet sample under the microscope lens; C) Processed picture of the microdroplets, outlining the circular area; D) Final picture isolating the microdroplet which circular outline can be measured accurately.

The three different microdroplet generators of Gen. 1 (Figure 23-B1, Annex 2), Gen. 2 (23-A1, Annex 2) and Gen. 3 (Figures 22-A1, 22-A2 and 22-A3, Annex 1) were tested regarding their capacity to pro-duce large amounts of monodisperse microdroplets. The results of the monodispersity experiments can be seen in Figures 9, 10 and 32 (Annex 5), for each of the generations. The results obtained demon-strated a validity for the third-generation devices to work in tandem with the previous generation devices as they encompass a significant range of possible microdroplet sizes, from 51 to 102 µm, and even focusing solely on the third-generation generation devices, it would be possible to obtain microdroplets with a range from 65 to 102 µm. The increase of the ratio between flow rates has an inverse proportion-ality relation with the size of microdroplets obtained, as expected from the principles that define how flow-focusing devices operate[102,111].
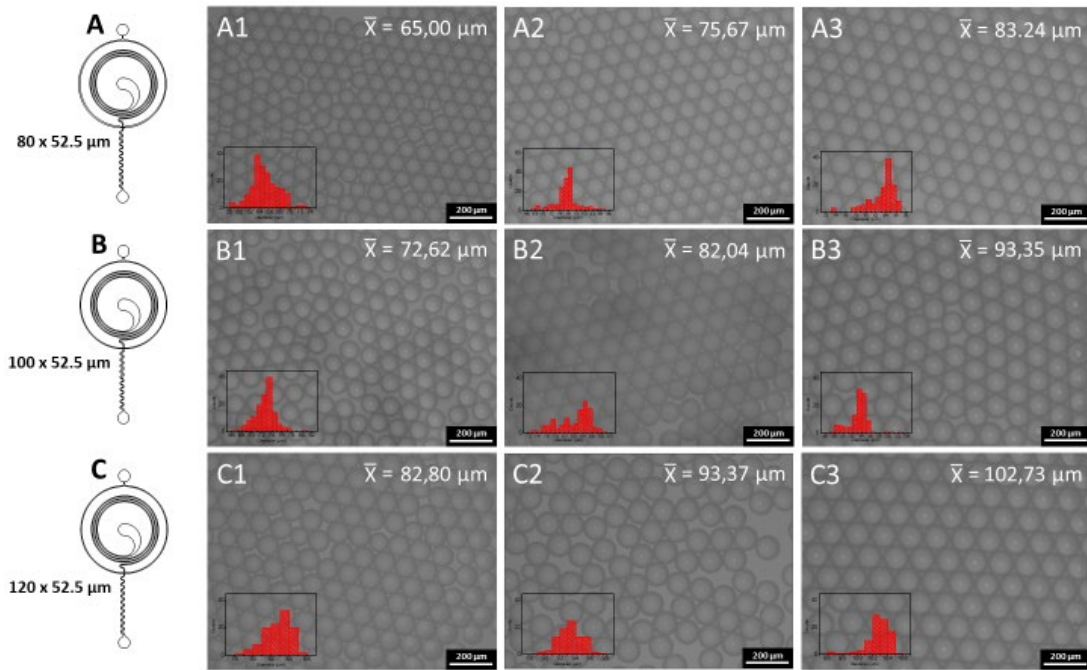
Figure 9 - Picture capture of the microdroplet samples under an optical microscope, produced by Gen. 3 devices with 80 μm (A), 100 μm (B) and 120 μm (C) t-section width, using Milli-Q as the dispersive phase and FC-40 + PS-1 as the continuous phase, followed by subsequent analysis regarding average size and size dispersion illustrated in the histograms placed on the bottom left corner of the pictures, with ratio values between the continuous and dispersive phases of 20 (A1, B1, C1), 10 (A2, B2, C2) and 5 (A3, B3, C3).
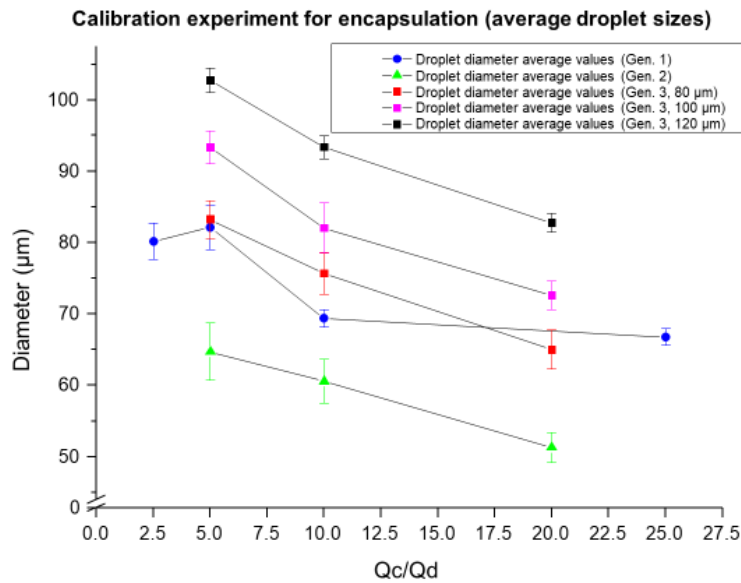
Figure 10 - Graph with the results of the experiments shown in Figure 9 depicting the differences between the average microdroplet sizes produced by the three microfluidic microdroplet generators (Gen. 1, Gen. 2 and Gen. 3) and different flow rate ratio values (Qc/Qd).

3.2.2 Microdroplet linear traps (Linear reservoir)

The linear reservoirs were analysed regarding the presence of traps in the resulting PDMS moulds obtained from soft lithography. Since there could be a chance that the features of the traps were too small to be replicated in the master, the three types of linear reservoirs with traps of 80, 100 and 120 µm were tested to see if the traps were present in the PDMS moulds and if they endured the constant passage of microdroplets through direct contact and with different flow rates without deforming. The results of the stability of the trap structures can be found in Figure 11.
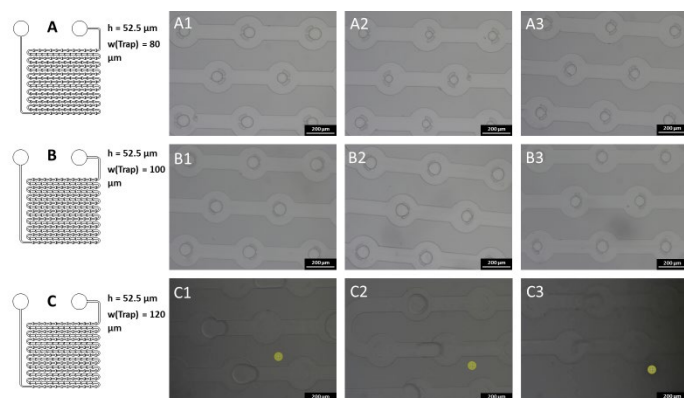
Figure 11 – AutoCAD designs and picture capture of the linear reservoir traps with 80 µm (A), 100 µm (B) and 120 µm (C) width under optical microscopy using Milli-Q as the dispersive phase and FC-40 + PS-1 as the continuous phase. The pictures represent the behaviour of the traps holding the microdroplets in place with flow rates specified for the dispersive phase and for the continuous phase, with the dispersive phase stable at 100 µL h^{-1} for all experiments and with three values for the continuous phase of 500 µL h^{-1} (A1, B1, C1), 1000 µL h-1 (A2, B2, C2) and 2000 µL h^{-1} (A3, B3, C3).

Based on the preliminary results shown in Figure 11, the linear reservoir moulds with 80 and 100 µm appear functional enough to hold microdroplets in place even after increasing the flow rate of the continuous phase. As the flow rate of the continuous increases, the microdroplets acquire enough motion to squeeze through the opening in the middle of the traps, due to the reduced size of microdroplets and increased pressure in the traps[59]. The results for the linear reservoir moulds with 120 µm traps revealed that the microdroplets do not hold in the designated trap zones, which indicated that the traps, although with the trap marks distinguished clearly, do not have thickness enough to form rigid trap structures in the PDMS moulds. This could be attributed to the design of the traps being too thin to be properly developed in the wafer, resulting in their removal by excessive erosion.

3.3 Durability of microdroplets

The durability of microdroplets was a major point of focus for the thesis, since the durability was crucial to perform long-term testing of cell growth. Several characteristics have been studied, but eventually only three were selected to observe which combination would provide the best conditions for microdroplets to endure. The type of oil used for the continuous phase (with PS-1 incorporated) and the method to proceed with the sealing of the device were altered throughout the thesis to adjust to emerging adverse factors that appeared.

3.3.1 Continuous phase composition

Two different types of oils were considered for microdroplet generation: HFE 7500 and FC-40, both incorporated with the surfactant PS-1 in 1 % of total volume. The first experiments of the thesis relied solely on HFE 7500, since the focus on those experiments was in producing monodisperse micro-droplets. But as the experiments advanced to long-term monitoring of microdroplets in enclosed reservoirs, the reservoirs could not impede the infiltration of air through the inlets for more than two days after the sealing was executed when using HFE 7500, as demonstrated in Figure 12.

Faced with the results obtained, the decision was made to attempt to switch from HFE 7500 oil to FC-40, which has reportedly guaranteed[124]. Previous articles have demonstrated that the FC-40 oil does have the potential of avoiding the infiltration of air into the reservoir[93]. For the purpose of ensuring that no random events are determinant in the success of specific experiments, it was decided that all experiments would be made once and then replicated once to confirm if the results obtained for both are similar in nature.

Based on the results obtained for the use of FC-40 in Figure 13, it was decided that FC-40 would be the best choice for the continuous phase to ensure long-term durability of droplets, while maintaining air infiltration into the device.
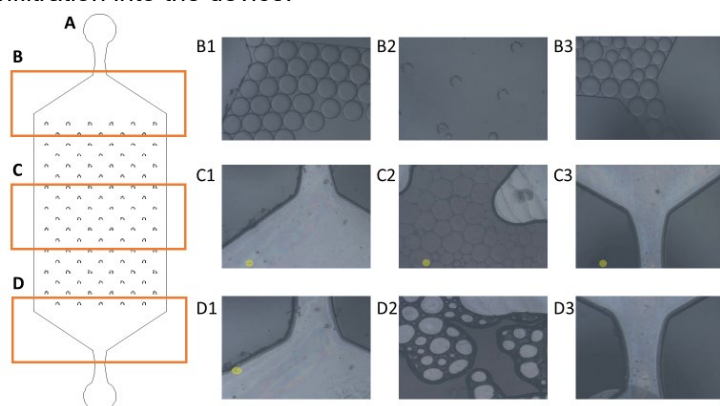
Figure 12 - Results of the encapsulation experiments for microdroplet durability, obtained by optical microscopy, and daily observation of the closing of the Gen. 1 reservoirs (A), using Milli-Q as the dispersive phase and HFE 7500 + PS-1 as the continuous phase, in three specific regions: upper inlet (B), middle (C) and lower inlet (D). The pictures for the experiment were taken within three time periods: day 0 (B1, B2, B3), day 1 (C1, C2, C3) and day 2 (D1, D2, D3).
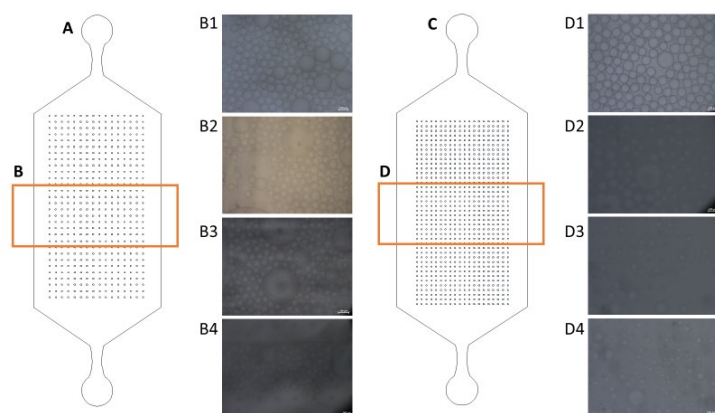
Figure 13 - Results of the encapsulation experiments for microdroplet durability, obtained by optical microscopy, and weekly observation of the closing of the Gen. 1 reservoirs with pillars spaced 150 µm (A) and 100 µm (B) in the middle region of the devices (C, D), using Milli-Q as the dispersive phase and FC-40 + PS-1 as the continuous phase. The pictures of the experiment were taken within four time periods: day 0 (B1, D1), day 7 (B2, D2), day 14 (B3, D3) and day 21 (B4, D4).

3.4 Cell encapsulation efficiency

The process of single cell encapsulation can be seen a random event in time, in which the generation of droplets with cells can follow a Bernoulli trial given that during the event of a cell being encapsulated into a microdroplet it is implied that it is very unlikely that two cells occupy the same physical space, thus single cell encapsulation can be considered as a case of "success", while empty droplets can be classified as "failure"[125]. However, for this thesis, we consider to be more cases of success for multiple cell encapsulations.

It is possible can summarize the probability of calculating how many cells can be encapsulated in a droplet by means of a Poisson distribution formula[126] if the number of events takes on discrete values Thus, the formula in Equation 1.1. can be used for cell encapsulation rates, based on Poisson distribution:

Equation 1.1.[125] $$P(Xc = k) = \ e^{-\lambda} \frac{\lambda^k}{k!}$$

The random variable, Xc, takes on the form of k, which represents the number of events taking place in a given interval, which can be considered by context as the number of cells that can be encapsulated in the specified volume of a droplet, and λ is the average number of cells encapsulated given a specified volume, which can be calculated according to Equation 1.2:

Equation 1.2.[126] $$\lambda = \ \frac{\phi s}{\phi d}$$

The variable ϕs represents the number of cells in the cell solution and the variable ϕd represents the number of droplets that can be made with a given volume of solution entering the microfluidic device. For the sake of simplicity, the volume for the solution with the cells and for droplet generation will be 1 mL, so Equation 1.2. can still be simplified into Equations 1.3. and Equation 1.4.:

Equation 1.3. $$\phi s = \ \frac{number\ of\ cells}{1\ mL}$$

Equation 1.4. $$\phi d = \ \frac{1\ mL}{\frac{4}{3}\pi r^3}$$

The cell density is calculated previously during cell culture growth being a known value. The volume of a droplet, can be calculated after encapsulating cells in droplets as an average value, using ImageJ as described in Figure 8 (chapter 3.2).

The focus of this thesis resides in observing single cancer cells growing and multiplying within microdroplets, so it is preferred that single cell encapsulations take place more frequently than multiple cell

encapsulations[127]. Dean flow architecture attempts to attenuate the occurrence of multiple cell encapsulations by "separating" the cells more evenly, by pushing the cells to the outer walls of the microfluidic channels as they travel to the T-section[59,113,114]. And using flow-focusing device principles, the frequency with which microdroplets are formed can be controlled by adjusting the flow rate of the continuous phase. The main objective for the cell encapsulation experiments was to observe if the Gen. 3 microdroplet generator devices can obtain higher cell encapsulation values than those expected by Poisson distribution.

Due to constraints in the production of the master designed for this thesis, this part of thesis was done resorting to the Gen. 2 Dean flow devices since the Dean flow geometry applied to the channel for the dispersive phase was very similar to the Gen. 3 Dean flow devices. An assumption was formulated, in which the values for the encapsulation rates between the Gen.2 and Gen. 3 devices were considered approximate due to similarities in geometry and channel size. For the cell encapsulation experiments, three different cell densities were utilized and three different flow rates for the continuous phase were applied, making for a total of 9 cell encapsulation experiments, as depicted in Figure 14 and Table 2, which represent an illustration of the setup for the experiments and a matrix for the combination of possible experiments. For the 1M (1 million, M = million) cell density solution, MDA-MB-435S (MDA) cells were utilized, and for the 2M and 3M experiments, SK-BR-3 cells were utilized. This decision was only based on the scarcity of cell cultures, not deliberately. This change presumedly bears no influence in encapsulation rates even if the cell solutions had all the same type of cells.

Table 2 - Matrix of combinations indicating the number of cell encapsulation experiments that were performed and the different conditions for each experiment.

		Cell density values:		
		1 million cells mL^{-1}	2 million cells mL^{-1}	3 million cells mL^{-1}
Continuous flow rates:	2000 µL h^{-1}	2000 µL h^{-1} x 100 µL h^{-1} at 1M	2000 µL h^{-1} x 100 µL h^{-1} at 2M	2000 µL h^{-1} x 100 µL h^{-1} at 3M
	1000 µL h^{-1}	1000 µL h^{-1} x 100 µL h^{-1} at 1M	1000 µL h^{-1} x 100 µL h^{-1} at 2M	1000 µL h^{-1} x 100 µL h^{-1} at 3M
	500 µL h^{-1}	500 µL h^{-1} x 100 µL h^{-1} at 1M	500 µL h^{-1} x 100 µL h^{-1} at 2M	500 µL h^{-1} x 100 µL h^{-1} at 3M

Dispersive phase flow rate (for all experiments): 100 µL h^{-1}

Syringe pump for **FC-40 + PS-1** (500, 1000, 2000 µL h^{-1} flow rates)

80µm

Glass slide

Syringe tubing (500 µm diameter)

Syringe pump for **MDA-MB-435** (for 1M solutions) or **SK-BR-3** (for 2M and 3M solutions) **+ PBS** (100 µL h^{-1} flow rate)
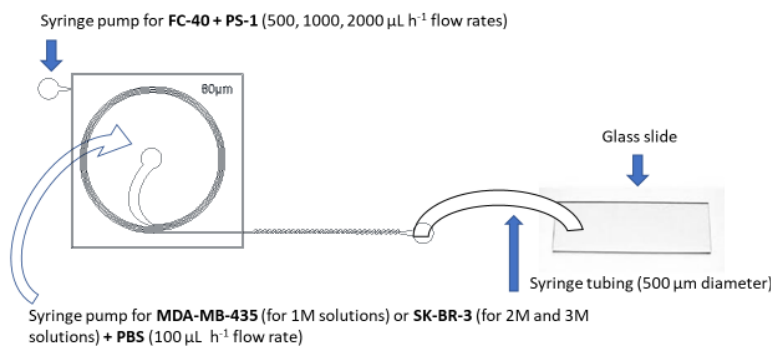
Figure 14 - Experiment layout with device placement and solutions utilized (glass slide is placed under the microscope for image acquisition).

The results for the nine cell encapsulation experiments can be found in Annex 7, for Figure 36. A minimum of 100 analysed microdroplets was established for all experiments, and in order to simplify calculations, any microdroplet with more than 1 cell encapsulated was considered as a multiple cell encapsulation event. Figure 15 illustrates the comparison[113] of the experimental values obtained with the theoretical values calculated using the Poisson distribution formula described in Equation 1.1..
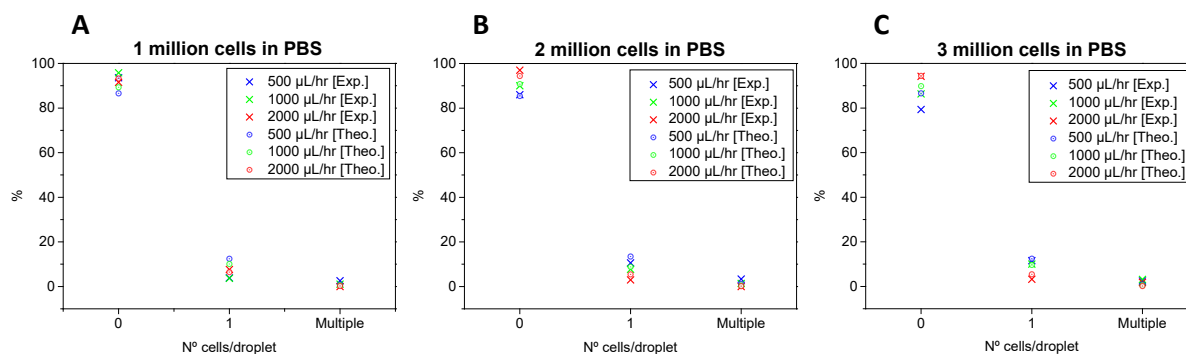
Figure 15 - Cell encapsulation efficiency results exhibited in 3 different graphs illustrating the comparison between the experimental results (cross shapes) and the theoretical calculations (centre-pointed transparent circle shapes) for each of the three different cell solutions: 1 × 10^6 cells mL^-1 (A), 2 × 10^6 cells mL^-1 (B) and 3 × 10^6 cells mL^-1 (C).

The graphs illustrate that no specific combination of the three continuous flow rates with the three cell density solutions could generate a population of microdroplets in which single cell encapsulation rates could surpass the values predicted by Poisson distribution[74,113]. The highest value obtained in percentage for single cell encapsulation was 11.57 %, for the experiment with the continuous phase flow rate at 500 µL h^-1 and cell density of 3×10^6 cells mL^-1 for the dispersive phase solution. That experiment also registered the lowest empty microdroplet count, at 79.34 %, which indicated that this specific combination might be the one more indicated to maximize the probabilities of obtaining single cell encapsulation events in further experiments[93].

3.5 Cell growth proliferation in microdroplets

The experiments for cell encapsulation and monitoring were performed for several days, under different conditions. A summary of each experiment was included in sub-sections of this chapter for further appreciation.

Table 3 contains a layout of the type of microdroplet generators and reservoirs used for droplet and cell incubation, the contents of the dispersive phase (cell density) and the flow rates used for each experiment within the complete set for each round. Each experiment was performed in replicates, filling 2 reservoirs each, to ensure a higher rate of success. A more detailed report of this chapter was placed in Annex 9 due to limitations in the total number of pages available, with emphasis in number of reservoirs sealed, how many were considered for analysis and considerations in distinguishing cancer cells in optical microscopy.

Table 3 - Layout of the performed sets of experiments for cell encapsulation and subsequent monitoring (yellow cells stand for deliberate modification to those factors for set to set; orange cells stand for modifications that were made on the spot due to unexpected complications).

Set	Device	% MG	Cell density (cells mL^{-1})	Flow rates ($Q_{cont.} \times Q_{disp.}$) *	Days
1	**Gen. 3** Dean flow microdroplet generator (80 μm width); **Gen. 3** Linear reservoir (80, 100 μm);	1, 2, 4, 8	2 × 10^6	500 x 100 μL h^{-1}	4-7
2	**Gen. 3** Dean flow microdroplet generator (80 μm width); **Gen. 3** Linear reservoir (80, 100 μm);	4	1 × 10^6 3 × 10^6 5 × 10^6	500 x 100 μL h^{-1}	2-4
3	**Gen. 3** Dean flow microdroplet generator (80 μm width); **Gen. 1** Open-spaced reservoir with traps (60, 80, 100 μm);	1, 2, 4, 8	2 × 10^6	500 x 100 μL h^{-1}	6-9
4	**Gen. 1** Flow focusing microdroplet generator (100 μm width); **Gen. 1** Open-spaced reservoir with traps (60, 80, 100 μm diameter), glass and PDMS bottom layer	1, 2, 4, 8	2 × 10^6	1000 x 100 μL h^{-1}	5
5	**Gen. 1** Flow focusing microdroplet generator (100 μm width); **Gen. 1** Open-spaced reservoir with traps (60, 80, 100 μm), functionalized and non-functionalized;	2, 4, 8	1 × 10^6	1000 x 100 μL h^{-1}	9-13

*$Q_{cont.}$ – *Continuous phase flow rate;* $Q_{disp.}$ – *Dispersive phase flow rate; MG: Matrigel®*

3.5.1 Results of the 1ˢᵗ set

Microdroplets were counted individually as regarding to their contents and their diameter, in order to sort them according to the number of cells they hold and compare them theoretically to the expected values under Poisson's distribution, depending on the values obtained for the average diameter of the microdroplets counted. The reservoirs were monitored for several days, even after all microdroplets had collapsed or evaporated, so the last image available for each reservoir represents a "blank" reservoir with no discernible parameter to analyse, and so those pictures will not present any tables to describe their contents.

For this chapter, a few images were selected along with close-ups of specific zones of the reservoirs to identify certain microdroplets that appear to have not just MDA cells encapsulated within, but also in a state of activity that may suggest an attempt of division and multiplication.

Table 4 – Layout of the 1st set of experiments executed for cell encapsulation and subsequent monitoring (after execution).

Condition	Device	Reservoir	Dispersive phase	Cell density (cells mL^{-1})	Flow rates ($Q_{cont.} \times Q_{disp.}$) *
1		**Gen. 3** Linear reservoirs 100 µm	**MDA-MB-435** cells + DMEM + 1 % Matrigel®		
2	**Gen. 3** Dean flow 80 µm	**Gen. 3** Linear reservoirs 100 µm	**MDA-MB-435** cells + DMEM + 2 % Matrigel®	2×10^6	500 x 100 µL h^{-1}
3		**Gen. 3** Linear reservoirs 80 µm	**MDA-MB-435** cells + DMEM + 4 % Matrigel®		
4		**Gen. 3** Linear reservoirs 80 µm	**MDA-MB-435** cells + DMEM + 8 % Matrigel®		

$Q_{cont.}$ – Continuous phase flow rate; $Q_{disp.}$ – Dispersive phase flow rate;

The first noticeable result consists in the feasibility of encapsulating droplets with any of the four different percentages of Matrigel®, indicated that the current method of adding Matrigel® to the dispersive phase appears to be functional enough to apply to further studies. To the best of our knowledge[74,119], this is the first the first time that microdroplets containing Matrigel® were generated with Matrigel® in direct contact with the interface of the microdroplets, being a step forward towards the proliferation of cells in droplets, and even towards cell to cell interaction mechanism at a local and restricted level.

Most of the results obtained 63 h after sealing the reservoirs was underwhelming, having most reservoirs suffered from air infiltration, low microdroplet formation and mass collapse of microdroplets throughout the channels[107]. The original purpose of retaining the droplets in the traps has proven unsuccessful, since the entrance of air pushes the contents of the channels to either direction, dragging the droplets to either of the inlets, depending from which inlet the air seems to be entering from. One possibility as to the incapacity of retaining the microdroplets in the same place may have to do with the way the reservoirs are placed in the plastic boxes as described in chapter 2.3.2. The box with the reservoirs had to be carried by hand to the CCL, and even assuming the utmost care in the transportation, the microdroplets could have moved by the slightest tilt of the hand, since the contents after sealed are governed by small variations in the pressure of the channels[103].

The only noticeable results appear with the reservoirs that have 4 % and 8 % of Matrigel® in the constitution of the dispersive phase. The air infiltration appears to be slower in reservoirs with 4 % and 8 % Matrigel®, which became a factor to be considered in further sets of experiments. As for the loss of monodispersity, numerous actors may have contributed to it, but most importantly was the accumulation of fibres throughout the channel, especially in the first traps where the microdroplets entered through, causing droplet splitting.
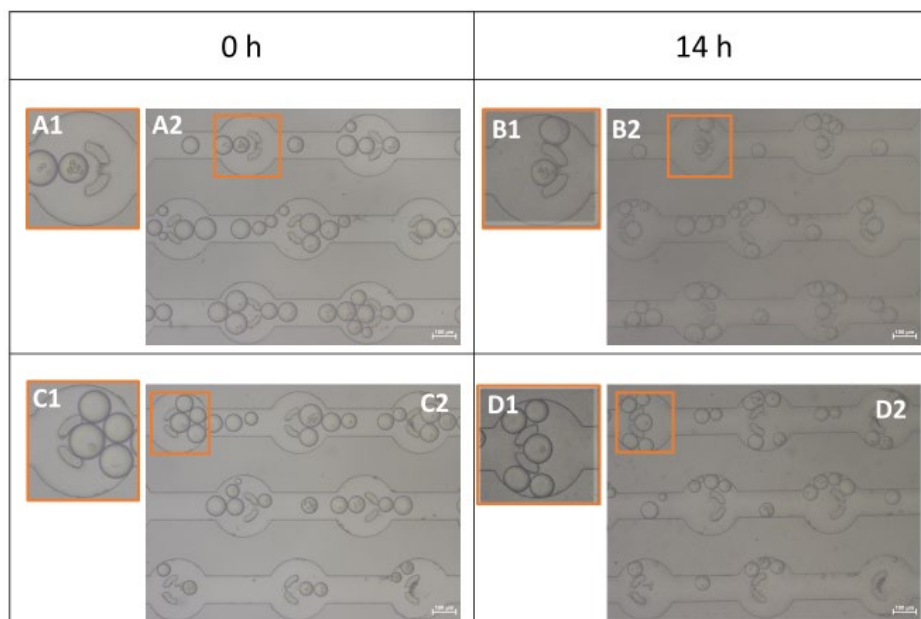
Figure 16 – Close-up pictures of microdroplets with cells encapsulated in Reservoir 1 with 4 % Matrigel® (A1, B1, C1, D1) from two instances in time: at the moment of sealing (A2, C2) and 14h after sealing (B2, D2).

In Reservoir 1 of condition 3, there were two instances in which the linear reservoirs managed to keep at least 1 microdroplet in the traps, allowing for a long-term observation from the moment they were encapsulated up to 14h, as illustrated in Figure 16.

Based on the results of the first set of experiments in Annex 7, the experiments with 4 % and 8 % Matrigel® appear to last longer than most, so both these values for Matrigel® percentage in the dispersive phase solution will be kept under consideration.

3.5.2 Results of the 2nd set

Table 5 – Layout of the 2nd set of experiments executed for cell encapsulation and subsequent monitoring.

Condition	Device	Reservoir	Dispersive phase	Cell density (cells mL^{-1})	Flow rates ($Q_{cont.} \times Q_{disp.}$) *
1	**Gen. 3** Dean flow 80 µm	**Gen. 3** Linear reservoir 80 µm, 17 rows	**MDA-MB-435** cells + DMEM + 4 % Matrigel®	1×10^6	500 x 100 µL h^{-1}
2		**Gen. 3** Linear reservoir 100 µm, 17 rows		3×10^6	
3		**Gen. 3** Linear reservoir 80 µm, 17 rows		5×10^6	

$Q_{cont.}$ – Continuous phase flow rate; $Q_{disp.}$ – Dispersive phase flow rate.

For the 2nd set of experiments, the focus of the experiments was to study the effects of how the increase in cell density would affect the overall process for cell encapsulation and observation of potential proliferation: encapsulation rates, comparison with the theoretical values based on Poisson distribution, microdroplet stability and evidence of growth within microdroplets with 1 cell or more. Initially the 2nd set was planned to have a durability of at least 1 week, but the reservoirs showed signs of air infiltration on day 1, so aspects such as microdroplet stability and cell growth were discarded, and the analysis of this set was then refocused on the encapsulation rates, average sizes for microdroplets and theoretical *vs* practical comparison. After extrapolating results from the 1st set of experiments, it was observed that the experiments with 4 % Matrigel® held the highest stability for microdroplets. Based on that observation, it was decided that the Matrigel® percentage for all experiments of the 2nd set would be set at 4 %. Analysing the results obtained for Set 2, the experiments from Conditions 1 and 3 presented more visibly impressive results, but while microdroplets made from solutions with 5×10^6 cells mL^{-1} had higher counts of producing more multicellular microdroplets (more than 5 cells per microdroplets), the results from Condition 1 showed that the experimental results obtained were closer to surpass Poisson distribution rates in single cell encapsulation than in the other experiments for Conditions 2 and 3. However, it was decided to remain using cell density values of 2×10^6 cells mL^{-1} for all other sets of experiments to limit the appearance of empty microdroplets.

3.5.3 Results of the 3rd set

Unfortunately, at the start of the 3rd set of experiments, the wafer with the Gen. 3 devices (Annex 1) had been compromised, forcing for the use of Gen. 1 reservoirs (Annex 2) to make up for the lack of available Gen. 2 and Gen. 3 reservoirs at the lab. However, there were still some Gen. 3 Dean flow droplet generators that still worked, so for the time being those would be the designated droplet generators.

Table 6 - Layout of the 3rd set of experiments executed for cell encapsulation and subsequent monitoring.

Condition	Device	Reservoir	Dispersive phase	Cell density (cells mL^{-1})	Flow rates ($Q_{cont.} \times Q_{disp.}$) *
1	**Gen. 3** Dean flow 80 μm	**Gen. 1** Trap reservoirs (80, 100, 120 μm)	**MDA-MB-435** cells + DMEM + 1 % Matrigel®	2×10^6	500 x 100 μL h^{-1}
2			**MDA-MB-435** cells + DMEM + 2 % Matrigel®		
3			**MDA-MB-435** cells + DMEM + 4 % Matrigel®		
4			**MDA-MB-435** cells + DMEM + 8 % Matrigel®		

$Q_{cont.}$ – Continuous phase flow rate; $Q_{disp.}$ – Dispersive phase flow rate.

The results of this set of experiments centred around 2 specific occurrences: great loss of visibility of the microdroplet contents 131 h after sealing and apparent signs of cell aggregation. As noticed by previous experiments from Sets 1 and 2, the viewing conditions tend to become aggravated after a few hours in the incubator. A possible cause for this may be the diffusion of water through the PDMS. Despite these difficulties, at the end of this set of experiments, two experiments produced noticeable results: Reservoir 2 with 2 % Matrigel® and Reservoir 2 with 4 % Matrigel®. Figure 17 exhibits close-ups of microdroplets with cells from the reservoirs, in order to present a concrete notion of their stability throughout time periods and alterations in their contents.

MG/Time	0 h	41 h	131 h	187 h
2 %, reservoir 2	A1	A2	A3	A4
4 %, reservoir 2	B1	B2	B3	B4
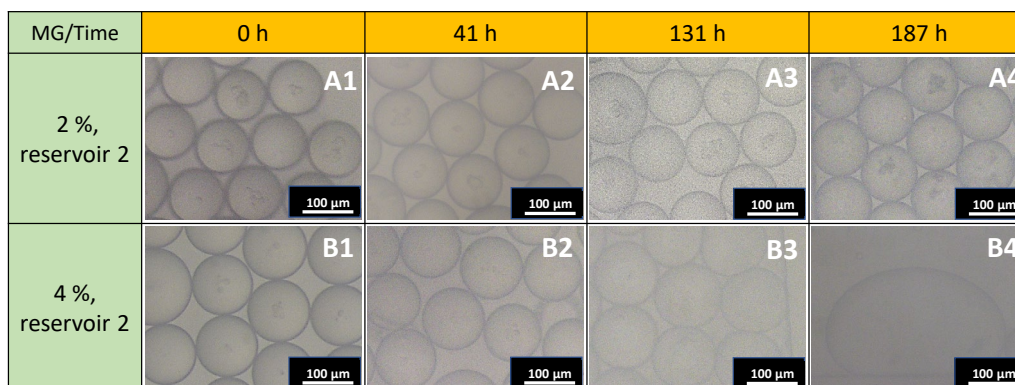
Figure 17 - Close-up of microdroplets from results of the Set 3 of experiments with the longest time elapsed, with pictures from different times regarding sealing procedures: at the moment of sealing (A1, B1), 41 h later (A2, B2), 131 h later (A3, B3) and 187 h later (A4, B4).

The results obtained demonstrate that the microdroplets can withstand long periods of time without collapsing or merging into bigger microdroplets. When microdroplets start incorporating too many cells, those cells have to pack further into the microdroplet, making them harder to count by means of a microscope without confocal lens for multiple plane observation. As it can be noticed, from the 131 h pictures after some time the contents of the microdroplets become difficult to discern due to the presence of "haze", having to modify the pictures using specific software. During the experiments, an idea was explored as to the use of glass as a bottom layer material for the reservoirs, in the hopes in increasing the visibility after several days, which was adopted in the next set of experiments.

3.5.4 Results of the 4th set

For the 4th set of experiments, **two different types of bottom layer were used to form the reservoirs: PDMS and glass**. The objective for this experiment was to observe if there would be notorious differences in the visualization of droplets after several hours had passed. Another factor that was to be analysed was the frequency of air infiltration with different layers, to see if there is an offset in each one of the two materials up for consideration[128]. Assumedly, since the droplet generator device had to be switched by another with a larger T-section (due to the unexpected unavailability of the mould with Gen.3 devices), it would be expected the average size of droplets to be bigger than the average sizes obtained in previous tests. However, as the focus of this set was in assessing viewing issues, the circumstance

of bigger droplet size will not be brought forth for discussion. One particular trick was used in an attempt to improve visibility of the reservoirs in subsequent observations after the sealing of the reservoirs. While adjusting the bright/dark filed settings of the microscope, the valve was placed in between the switch from bright to dark, permitting the accentuation of the features of the microdroplets to overcome the "haze" that appears after a few hours in the incubator. Out of all the experiments made, four of the reservoirs had very interesting results in terms of microdroplet stability, having the close-ups of those results exhibited in Figure 18.

Table 7 – Layout of the 4th set of experiments executed for cell encapsulation and subsequent monitoring.

Condition	Microdroplet generator	Reservoir	Dispersive phase	Cell density (cells mL^{-1})	Flow rates ($Q_{cont.} \times Q_{disp.}$)*
1		**Gen. 1** Trap reservoirs (80, 100, 120 µm), Glass Layer	**MDA-MB-435** cells + DMEM + 1 % Matrigel®		
2		**Gen. 1** Trap reservoirs (80, 100, 120 µm), PDMS layer	**MDA-MB-435** cells + DMEM + 1 % Matrigel®		
3		**Gen. 1** Trap reservoirs (80, 100, 120 µm), Glass Layer	**MDA-MB-435** cells + DMEM + 2 % Matrigel®		
4	**Gen. 1** Flow-Focusing device, 100 µm width	**Gen. 1** Trap reservoirs (80, 100, 120 µm), PDMS Layer	**MDA-MB-435** cells + DMEM + 2 % Matrigel®	2×10^6	1000 x 100 µL h^{-1}
5		**Gen. 1** Trap reservoirs (80, 100, 120 µm), Glass Layer	**MDA-MB-435** cells + DMEM + 4 % Matrigel®		
6		**Gen. 1** Trap reservoirs (80, 100, 120 µm), PDMS Layer	**MDA-MB-435** cells + DMEM + 4 % Matrigel®		
7		**Gen. 1** Trap reservoirs (80, 100, 120 µm), Glass Layer	**MDA-MB-435** cells + DMEM + 8 % Matrigel®		
8		**Gen. 1** Trap reservoirs (80, 100, 120 µm), PDMS Layer	**MDA-MB-435** cells + DMEM + 8 % Matrigel®		

$Q_{cont.}$ – Continuous phase flow rate; $Q_{disp.}$ – Dispersive phase flow rate
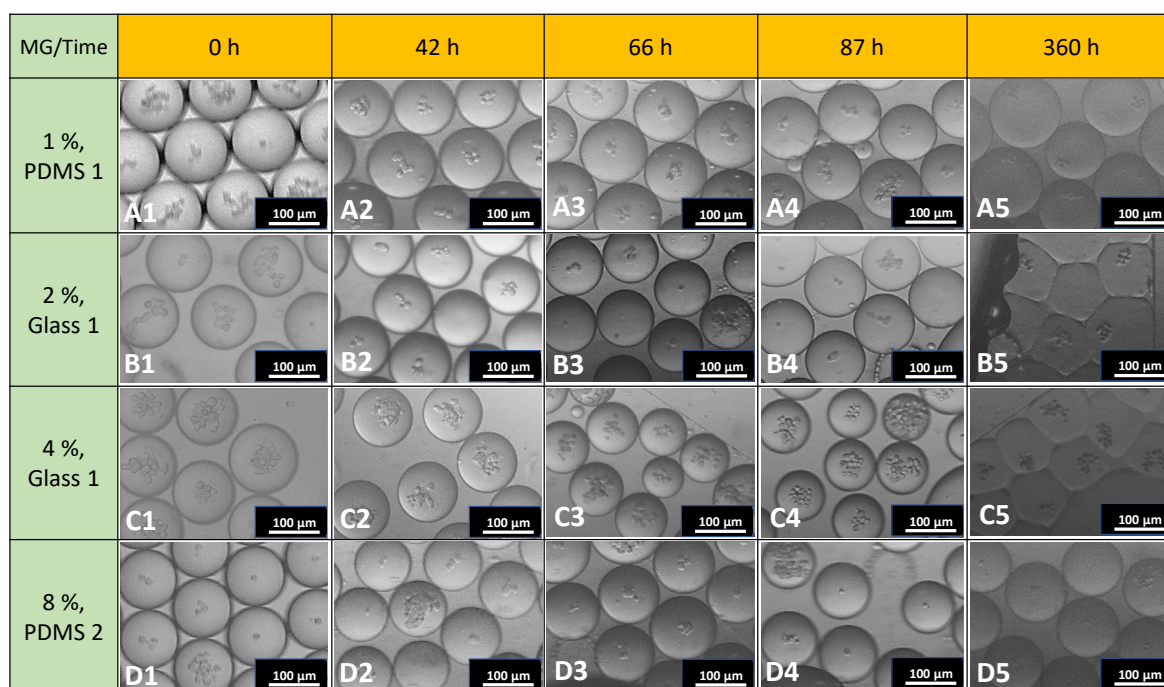
Figure 18 - Experimental results of the 4th set for the four of the reservoirs with the longest longevity per each of the four categories regarding Matrigel® percentage. Pictures at different times regarding sealing procedures: at the moment of sealing (A1, B1, C1, D1), 42 h later (A2, B2, C2, D2), 66 h later (A3, B3, C3, D3), 87 h later (A4, B4, C4, D4) and 360 h later (A5, B5, C5, D5).

Based on the qualitative analysis of all the experiments from this set, the reservoirs with the bottom layer of glass tend to suffer from air infiltration faster than those done with a PDMS layer, but in terms of visibility, glass layers provide better visibility for longer time. However, it is worth noting that the visibility appears to be adequate for all types of reservoirs with the new microscope set up suing dark filed mode, indicating that the adjustment in the bright/dark field settings appears to be effective to allow a proper analysis of the contents in microdroplets. Since there is a preference in maintaining the microdroplets stable for longer periods of time, it was decided to continue using PDMS as a bottom layer material rather than glass.

3.5.5 Results of the 5th set

The final set of experiments was conceived in order to analyse if the current batch of Aquapel® was compromised, due to repeated events of microdroplet collapse throughout all the sets of experiments. Due to the low remarks seen in the previous sets, the use of solutions with 1 % Matrigel® for the dispersive phase was discontinued, resorting only to 2 %, 4 % and 8 % solutions for this set. Due to constraints in time, the only parameters subject to analysis in this set were the average droplet size and the overall stability throughout several days.

The results of the 5th set are presented in Figures 19 and 20, with close-ups of the microdroplets placed in.

Table 8 - Layout of the 5th set of experiments executed for cell encapsulation and subsequent monitoring.

Condition	Microdroplet generator	Reservoir	Dispersive phase	Cell density (cells mL $^{-1}$)	Flow rates ($Q_{cont.} \times Q_{disp.}$)*
1	**Gen. 1** Flow-Focusing device, 100 µm width	**Gen. 1** Trap reservoirs (80, 100, 120 µm), functionalized	**MDA-MB-435** cells + DMEM + 2 % Matrigel®	1×10^6	1000 x 100 µL h^{-1}
2		**Gen. 1** Trap reservoirs (80, 100, 120 µm), non-functionalized	**MDA-MB-435** cells + DMEM + 2 % Matrigel®		
3		**Gen. 1** Trap reservoirs (80, 100, 120 µm), functionalized	**MDA-MB-435** cells + DMEM + 4 % Matrigel®		
4		**Gen. 1** Trap reservoirs (80, 100, 120 µm), non-functionalized	MDA-MB-435 cells + DMEM + 4 % Matrigel®		
5		**Gen. 1** Trap reservoirs (80, 100, 120 µm), functionalized	MDA-MB-435 cells + DMEM + 8 % Matrigel®		
6		**Gen. 1** Trap reservoirs (80, 100, 120 µm), non-functionalized	MDA-MB-435 cells + DMEM + 8 % Matrigel®		

*$Q_{cont.}$ – *Continuous phase flow rate;* $Q_{disp.}$ – *Dispersive phase flow rate;*
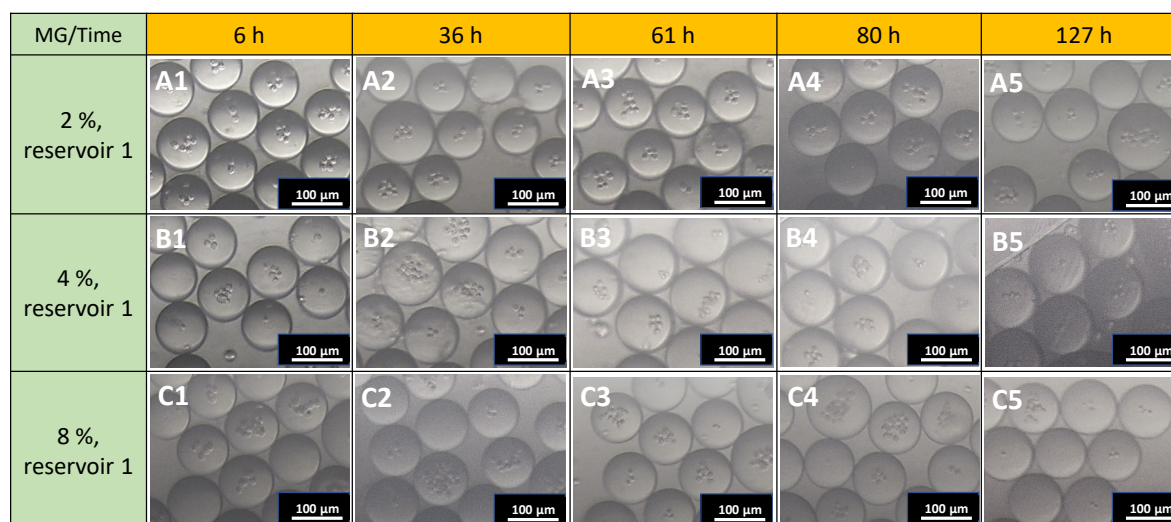
Figure 19 - Set 5 experimental results for the non-functionalized reservoirs with the longest longevity per each of the 3 categories regarding Matrigel® percentage. The pictures depict different times regarding sealing procedures: 6h after sealing (A1, B1, C1), 36 h later (A2, B2, C2), 61 h later (A3, B3, C3), 80 h later (A4, B4, C4) and 127 h later (A5, B5, C5).
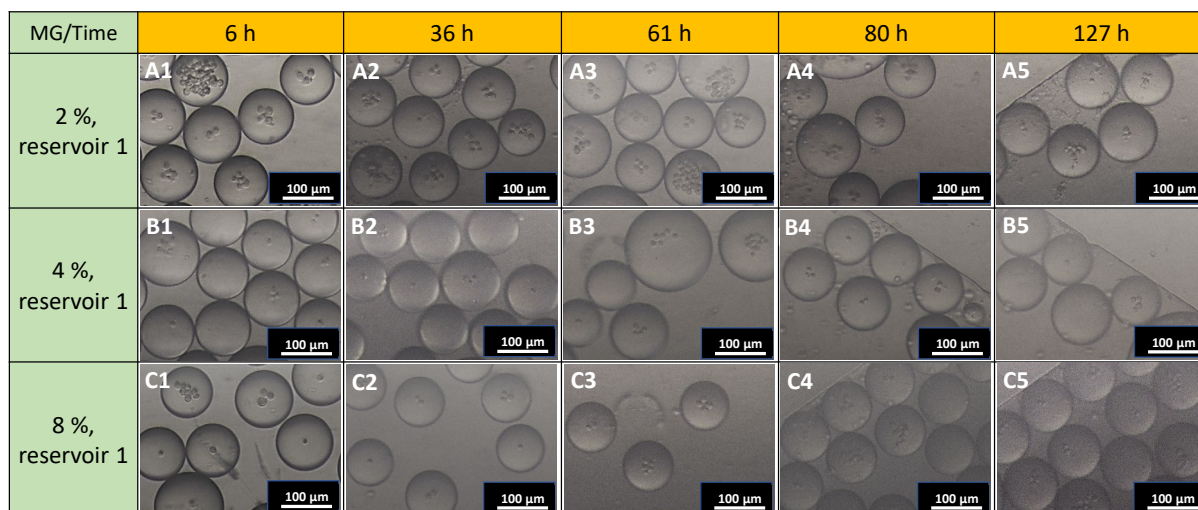
Figure 20 - Set 5 experimental results for the functionalized reservoirs with the longest longevity per each of the 3 categories regarding Matrigel® percentage. The pictures depict different times regarding sealing procedures: 6h after sealing (A1, B1, C1), 36 h later (A2, B2, C2), 61 h later (A3, B3, C3), 80 h later (A4, B4, C4) and 127 h later (A5, B5, C5).

The results in Figures 19 and 20 showed that the microdroplets maintained an acceptable stability for up to 5 days between the two types of reservoir treatments, which indicated that the Aquapel® might not be the cause of the instability that leads to the collapses.

3.5.6 Remarks about single-cell growth in microdroplets

The method for cell culture preparation used throughout this thesis was developed through multiple protocols between different articles regarding cell growth, with the compilation of all the important aspects summarized in Table 9 and with all the aspects in Table 10 in Annex 8.

Table 9 is a compilation of different cell growth protocols in several articles for microfluidic purposes or for low counts of starting numbers of cells, in an attempt to study which would be the best approach to permit the growth of cells in microdroplets in an isolating setting for long durability. The table is split into different factors between each articles: cell line used, starting number of cells, seeding method (96-well plates, plate culture, droplets, etc.), culture media, extracellular matrix surrogate (Regular cell culture media, hydrogel), volume available for cultures, incubating conditions, time given to grow and growth dynamics (how fast they grow). Between most of the articles, the use of an additional reagent to simulate the effects of the extracellular matrix was considered significantly important in promoting cell growth when intending to reduce the expected elapsed time for cell growth. The use of Matrigel® was put under consideration, since the other reagents were adjusted for the specific conditions in which the experiments were performed and Matrigel® did not require too much preparation to be implemented in the cell cultures[77,119].

Table 9 – Compiled table with the different articles which served as base for the cell culture developed for the thesis and the most significant parameters.

Method	Starting n cells	Cell type	Days of culture	Ref.
96-well plates	3000000	MDA-MB-435 S/SK-BR-3	24h	[83]
Hanging drop	10000	MCF-7	3 days	[77]
48-well plates	100000	MDA-MB-231	6 days	[84]
96-well plates	5000	MDA-MB-231	24h + 48h	[81]
Hanging drop	4000	MV3-melanoma	24h	[72]
Droplet encapsulation, with a distinct barrier between the bead and the spheroid medium	1 or more cells, cannot specify because the project did not try to ensure single cell encapsulation	MCF-7	Not specified, stablishes timelines based on core components, from 2 to 4 days	[119]
Aseptically cultured in T-25 cell culture flasks/multi-well cell culture plates	300000	MCF-7 and MDA-MB-231	4 days (24h + 24h + 48h)	[129]
96-well plates	5000 primary cells, or 1000-2000 intermediary cells	Head and Neck squamous cell carcinoma (HNSCC) extracted from patients	7-10 days	[130]
48 or 96-well plates	1000000-5000000	Peripheral blood mononuclear cells (PoBMC)	7 days, re-supplied with media each 3 days	[131]
100-mm Petri Dishes	Not specified	Human prostate cancer cell lines PC3 and LnCAP, human breast cancer cell lines MDA-MB-231 and MCF-7, and lung cancer cell line H460	Over 7 days	[69]
96-well standard microplates, 96F non-adherent microplates, spheroid microplates and specialized microwell formats	Not specified	Head neck cancer cells extracted from patients	Estimated time of 7 days	[24]

Regarding the duration of droplets obtained throughout this thesis, it was quite possible to obtain durations up to 21 days, which is a significant step forward when comparing to some noticeable values, from 8 to 14 days obtained in different reports in literature[119,124]. Also, considering that the droplets were sealed in very tight structures from the reservoirs, it is noteworthy to consider that this thesis permitted to extend the limits of understanding regarding the special limitations that droplets can endure without collapsing entirely for long periods of time.

Based on the results obtained throughout this thesis, the current methods for preparing cell culture for growth into 3D spheroids within microdroplets are adequate to obtain cell encapsulation in microdroplets and to promote signs of growth through cell aggregation. As to this date, this thesis was the first attempt ever towards the proliferation of single cancer cells into spheroids in microdroplets, and assuming that the preparation of the dispersive phase solutions was as simplified as possible, given enough preparation it is believed that this line of thinking of growing spheroids in droplets, is indeed possible. We believe that before we can achieve that overarching aim, a very controlled protocol and technology must be optimized, to which this thesis has remarkably contributed forward.

4 Conclusions and Future Perspectives

During this thesis, I have developed a methodology that may be applied to the growth of single-cells and their proliferation into spheroids. Despite not having achieved the overarching aim of single-cell proliferation in droplets, several meaningful contributions towards that goal were made:

- A set of microfluidic devices that allow the high-throughput encapsulation and monitoring of cells in droplets was designed and fabricated.

- The most appropriate parameters for single-cell proliferation and long-term incubation have been narrowed down by: fabricating, optimising and testing nearly 80 reservoirs and 50 droplet generators, etc; establishing a matrix of over 25 different conditions by varying key parameters; acquiring and analysing over 1000 images and over 15000 droplets (pictures in Annex 9 can give an impression of the amount of effort that it took to build the results from all reservoirs made, across several days).

- It is possible to encapsulate cancer single-cells in microdroplets with Matrigel® supplement.

- Cancer cells can be incubated in droplets and in microfluidic reservoirs up to 21 days.

The prospect of using microdroplets as a means of an observation platform for cell growth is indeed a noticeable achievement that could pave the way for an easy method to study the events that lead to the heterogeneity that cancer cells possess, how to predict the most probable outcome within a plethora of different phenotypes, etc. However, throughout the course of this thesis, it became apparent that in order to implement this concept into practice, extensive experimentation will be required into developing a cell growth protocol that could work with any given number of cells. A hypothesis for the lack of apparent cell growth might involve the buoyancy effect that the cells are subjected when encapsulated in the microdroplets, which might discourage their growth if there is not a stable condition that promotes cohesion between cells. This method is still in its initial stages and might require significant resources to generate the perfect combination that can best emulate the microenvironment in which cancer cells proliferate.

The notion of utilizing microdroplets as a means of growing single cells into spheroids does confer significant advantages to conventional methods of growing cells in lab, like allowing individual analysis of each spheroid without having to filter them previously and obtaining high-throughput results that can be analysed for statistics. However, considering the other issues that occurred during the thesis, this technique requires contributions from the different fields of science to solve the most pressing issues regarding the sealing process, the longevity of microdroplets in solution and the control of the encapsulation rates.

Ideally, this process must be optimized for single cell encapsulation if it is to be used for the generation of complex 3D structures like spheroids from CTCs, since CTCs have a low rate of survivability. To that

end, the best way to achieve that would be optimizing the cancer cell growth methods from which this thesis was based upon.

The field of microfluidics has already proven that the potential to simulate the *in vivo* conditions that better reflect the actual behaviour of tumours exists, and in a very efficient way. All that is missing is the necessary effort to develop smart strategies to deal with the reduced number of cells, but with the work of this thesis, it was proven that the cells can withstand the isolated environment of a microdroplet without dying and can induce aggregation (although not by single cell encapsulation), which can serve as evidence about the potential for this technique in creating spheroids.

The impact of the technology developed during this thesis and its future advances would be two-fold: understanding mechanisms behind metastasis at the molecular and cellular level, and developing novel technologies for the development of 3D cultures and spheroids for therapy screening. Altogether, despite this work being on its very first stages, I hope it will have a future impact on the society in terms of a more personalised medicine, decrease on animal use for drug testing, better prognosis and more controlled diagnosis, as well as prevention through prediction of potential proliferation patterns of single-cells related to their genotype and phenotype.

References

1. Ritchie, H. & Roser, M. Causes of Death. *OurWorldInData.org* (2019). Available at: https://ourworldindata.org/causes-of-death. (Accessed: 3rd November 2019)

2. Ferlay J, Ervik M, Lam F, Colombet M, Mery L, Piñeros M, Znaor A, Soerjomataram I, B. F. (2018). Global Cancer Observatory: Cancer Today. *International Agency for Research on Cancer.* (2018). Available at: https://gco.iarc.fr/today. (Accessed: 2nd August 2019)

3. Ferlay, J. *et al.* Estimating the global cancer incidence and mortality in 2018: GLOBOCAN sources and methods. *Int. J. Cancer* **144**, 1941–1953 (2019).

4. Bray, F. *et al.* Global cancer statistics 2018: GLOBOCAN estimates of incidence and mortality worldwide for 36 cancers in 185 countries. *CA. Cancer J. Clin.* **68**, 394–424 (2018).

5. Stringhini, S. & Guessous, I. The shift from heart disease to cancer as the leading cause of death in high-income countries: A social epidemiology perspective. *Annals of Internal Medicine* **169**, 877–879 (2018).

6. De Souza, J. A., Hunt, B., Asirwa, F. C., Adebamowo, C. & Lopes, G. Global health equity: Cancer care outcome disparities in high-, middle-, and low-income countries. *J. Clin. Oncol.* **34**, 6–13 (2016).

7. Seyfried, T. N., Huysentruyt, L. C. & Norman, A. On the origin of cancer metastasis. *Crit. Rev. Oncog.* **18**, 43–73 (2013).

8. Welch, D. R. & Hurst, D. R. Defining the Hallmarks of Metastasis. *Cancer Res.* **79**, 3011–3027 (2019).

9. Bernard, D. S. M., Farr, S. L. & Fang, Z. National estimates of out-of-pocket health care expenditure burdens among nonelderly adults with cancer: 2001 to 2008. *J. Clin. Oncol.* **29**, 2821–2826 (2011).

10. Ward, E. *et al.* Association of Insurance with Cancer Care Utilization and Outcomes. *CA. Cancer J. Clin.* **58**, 9–31 (2008).

11. Voda, A. I. & Bostan, I. Public health care financing and the costs of cancer care: A cross-national analysis. *Cancers (Basel).* **10**, 1–13 (2018).

12. Bheda, P. & Schneider, R. Epigenetics reloaded: the single-cell revolution. *Trends Cell Biol.* **24**, 712–723 (2014).

13. Costa, E. C. *et al.* 3D Tumour spheroids: an overview on the tools and techniques used for their analysis. *Biotechnol. Adv.* **34**, 1427–1441 (2016).

14. Provero, P. *et al.* Somatic mutability in cancer predicts the phenotypic relevance of germline mutations. *bioRxiv Genomics* 1–14 (2018). doi:10.1101/447862

15. Alexandrov, L. B. *et al.* Signatures of mutational processes in human cancer. *Nature* **500**, 415–421 (2013).

16. Greenman, C. *et al.* Patterns of somatic mutation in human cancer genomes. *Nature* **446**, 153–158 (2007).

17. Torgovnick, A. & Schumacher, B. DNA repair mechanisms in cancer development and therapy. *Front. Genet.* **6**, 1–15 (2015).

18. Brown, A. L., Li, M., Goncearenco, A. & Panchenko, A. R. Finding driver mutations in cancer: Elucidating the role of background mutational processes. *PLoS Comput. Biol.* **15**, e1006981 (2019).

19. Pfeifer, G. P. Environmental exposures and mutational patterns of cancer genomes. *Genome Med.* **2**, (2010).

20.   Tysnes, B. Bø. Tumour-initiating and -propagating cells: Cells that we would like to identify and control. *Neoplasia* **12**, 506–515 (2010).

21.   Dalton-Griffin, L. & Kellam, P. Infectious causes of cancer and their detection. *J. Biol.* **8**, 67 (2009).

22.   Mesri, E. A., Feitelson, M. A. & Munger, K. Human viral oncogenesis: A cancer hallmarks analysis. *Cell Host Microbe* **15**, 266–282 (2014).

23.   Hiley, C., de Bruin, E. C., McGranahan, N. & Swanton, C. Deciphering intraTumour heterogeneity and temporal acquisition of driver events to refine precision medicine. *Genome Biol.* **15**, 1–10 (2014).

24.   Kulasinghe, A. *et al.* Short term *ex-vivo* expansion of circulating head and neck tumour cells. *Oncotarget* **7**, (2016).

25.   Jolly, M. K. *et al.* Hybrid epithelial/mesenchymal phenotypes promote metastasis and therapy resistance across carcinomas. *Pharmacol. Ther.* **194**, 161–184 (2019).

26.   Sprouffske, K., Merlo, L. M. F., Gerrish, P. J., Maley, C. C. & Sniegowski, P. D. Cancer in light of experimental evolution. *Curr. Biol.* **22**, R762–R771 (2012).

27.   Lipinski, K. A. *et al.* Cancer Evolution and the Limits of Predictability in Precision Cancer Medicine. *Trends in Cancer* **2**, 49–63 (2016).

28.   Merlo, L. M. F., Pepper, J. W., Reid, B. J. & Maley, C. C. Cancer as an evolutionary and ecological process. *Nat. Rev. Cancer* **6**, 924–935 (2006).

29.   Kaare Christensen, K., E Johnson, T. & W Vaupel, J. The quest for genetic determinants of human longevity: Challenges and insights. *Nat. Rev. Genet.* **7**, 436–448 (2006).

30.   Lynch, M. *et al.* Genetic drift, selection and the evolution of the mutation rate. *Nat. Rev. Genet.* **17**, 704–714 (2016).

31.   Lynch, M. Rate, molecular spectrum, and consequences of human mutation. *Proc. Natl. Acad. Sci. U. S. A.* **107**, 961–968 (2010).

32.   Pastushenko, I. & Blanpain, C. EMT Transition States during Tumour Progression and Metastasis. *Trends Cell Biol.* **29**, 212–226 (2019).

33.   Jiang, W. G. *et al.* Tissue invasion and metastasis: Molecular, biological and clinical perspectives. *Semin. Cancer Biol.* **35**, S244–S275 (2015).

34.   Navin, N. E. & Hicks, J. Tracing the Tumour lineage. *Mol. Oncol.* **4**, 267–283 (2010).

35.   Huang, Q. *et al.* Nanotechnology-Based Strategies for Early Cancer Diagnosis Using Circulating Tumour Cells as a Liquid Biopsy. *Nanotheranostics* **2**, 21–41 (2017).

36.   Hanahan, D. & Weinberg, R. A. Hallmarks of cancer: The next generation. *Cell* **144**, 646–674 (2011).

37.   Yuan, S., Norgard, R. J. & Stanger, B. Z. Cellular Plasticity in Cancer. *Cancer Discov.* **9**, 837–851 (2019).

38.   Meacham, C. E. & Morrison, S. J. Tumour heterogeneity and cancer cell plasticity. *Nature* **501**, 328–337 (2013).

39.   Dagogo-Jack, I. & Shaw, A. T. Tumour heterogeneity and resistance to cancer therapies. *Nat. Rev. Clin. Oncol.* **15**, 81–94 (2018).

40.   Burrell, R. A., McGranahan, N., Bartek, J. & Swanton, C. The causes and consequences of genetic heterogeneity in cancer evolution. *Nature* **501**, 338–345 (2013).

41.   Kreso, A. & Dick, J. E. Evolution of the cancer stem cell model. *Cell Stem Cell* **14**, 275–291 (2014).

42.   Sarkar, S., Cohen, N., Sabhachandani, P. & Konry, T. Phenotypic drug profiling in droplet

microfluidics for better targeting of drug-resistant Tumours. *Lab Chip* **15**, 4441–4450 (2015).

43.   Feitelson, M. A. *et al.* Sustained proliferation in cancer: Mechanisms and novel therapeutic targets. *Semin. Cancer Biol.* **35**, S25–S54 (2015).

44.   da Silva-Diz, V., Lorenzo-Sanz, L., Bernat-Peguera, A., Lopez-Cerda, M. & Muñoz, P. Cancer cell plasticity: Impact on Tumour progression and therapy response. *Semin. Cancer Biol.* **53**, 48–58 (2018).

45.   Ashworth, T. R. A case of cancer in which cells similar to those in the tumours were seen in the blood after death. *Aust Med J.* **14**, 146 (1869).

46.   Cristofanilli, M. *et al.* Circulating Tumour cells, disease progression, and survival in metastatic breast cancer. *N. Engl. J. Med.* **351**, 781–791 (2004).

47.   Kowalik, A., Kowalewska, M. & Góźdź, S. Current approaches for avoiding the limitations of circulating Tumour cells detection methods—implications for diagnosis and treatment of patients with solid Tumours. *Translational Research* **185**, 58-84.e15 (2017).

48.   Tellez-Gabriel, M. *et al.* Circulating Tumour Cell-Derived Pre-Clinical Models for Personalized Medicine. *Cancers (Basel).* **11**, (2018).

49.   Liao, C. J. *et al.* Isolation of label-free and viable circulating tumour cells (CTCs) from blood samples of cancer patients through a two-step process: Negative selection-type immunomagnetic beads and spheroid cell culture-based cell isolation. *RSC Adv.* **7**, 29339–29349 (2017).

50.   Krebs, M. G., Hou, J. M., Ward, T. H., Blackhall, F. H. & Dive, C. Circulating tumour cells: Their utility in cancer management and predicting outcomes. *Ther. Adv. Med. Oncol.* **2**, 351–365 (2010).

51.   Moon, D. H., Lindsay, D. P., Hong, S. & Wang, A. Z. Clinical indications for, and the future of, circulating Tumour cells. *Adv. Drug Deliv. Rev.* **125**, 143–150 (2018).

52.   Zhao, R. *et al.* Expression and clinical relevance of epithelial and mesenchymal markers in circulating Tumour cells from colorectal cancer. *Oncotarget* **8**, 9293–9302 (2017).

53.   Neumann, M. H. D., Bender, S., Krahn, T. & Schlange, T. ctDNA and CTCs in Liquid Biopsy – Current Status and Where We Need to Progress. *Comput. Struct. Biotechnol. J.* **16**, 190–195 (2018).

54.   Di Meo, A., Bartlett, J., Cheng, Y., Pasic, M. D. & Yousef, G. M. Liquid biopsy: A step forward towards precision medicine in urologic malignancies. *Mol. Cancer* **16**, 1–14 (2017).

55.   Stott, S. L. *et al.* Isolation and characterization of circulating Tumour cells from patients with localized and metastatic prostate cancer. *Sci. Transl. Med.* **2**, (2010).

56.   Pantel, K. & Speicher, M. R. The biology of circulating Tumour cells. *Oncogene* **35**, 1216–1224 (2016).

57.   Palmirotta, R. *et al.* Liquid biopsy of cancer: a multimodal diagnostic tool in clinical oncology. *Ther. Adv. Med. Oncol.* **10**, 1758835918794630–1758835918794630 (2018).

58.   Abalde-Cela, S., Piairo, P. & Diéguez, L. The Significance of Circulating Tumour Cells in the Clinic. *Acta Cytol.* (2019). doi:10.1159/000495417

59.   Gossett, D. R. *et al.* Label-free cell separation and sorting in microfluidic systems. *Anal. Bioanal. Chem.* **397**, 3249–3267 (2010).

60.   K.E., S. & A.C., L. Circulating Tumour Cells: Overview and Opportunities in Cytology. *Adv. Anat. Pathol.* **26**, 56–63 (2019).

61.   Zhang, J., Chen, K. & Fan, Z. H. *Circulating Tumour Cell Isolation and Analysis*. *Advances in Clinical Chemistry* **75**, (Elsevier Inc., 2016).

62.   Mamdouhi, T., Twomey, J. D., McSweeney, K. M. & Zhang, B. Fugitives on the run: circulating

Tumour cells (CTCs) in metastatic diseases. *Cancer Metastasis Rev.* **38**, 297–305 (2019).

63. Pantel, K. & Res, C. A. P. Functional studies on viable circulating Tumour Cells. *Clin. Chem.* **62**, 328–334 (2016).

64. Alix-Panabières, C. & Pantel, K. Liquid biopsy in cancer patients: Advances in capturing viable CTCs for functional studies using the EPISPOT assay. *Expert Rev. Mol. Diagn.* **15**, 1411–1417 (2015).

65. Drahansky, M. *et al.* CTCs as Liquid Biopsy: Where Are We Now? *Intech* **i**, 13 (2016).

66. Dong, Y. *et al.* Microfluidics and circulating Tumour cells. *J. Mol. Diagnostics* **15**, 149–157 (2013).

67. Gupta, N. *et al.* Microfluidics-based 3D cell culture models: Utility in novel drug discovery and delivery research. *Bioeng. Transl. Med.* **1**, 63–81 (2016).

68. Celià-Terrassa, T. & Kang, Y. Distinctive properties of metastasis-initiating cells. *Genes Dev.* **30**, 892–908 (2016).

69. Kaushik, V., Yakisich, J. S., Way, L. F., Azad, N. & Iyer, A. K. V. Chemoresistance of cancer floating cells is independent of their ability to form 3D structures: Implications for anticancer drug screening. *J. Cell. Physiol.* **234**, 4445–4453 (2019).

70. Kim, S. A., Lee, E. K. & Kuh, H. J. Co-culture of 3D Tumour spheroids with fibroblasts as a model for epithelial-mesenchymal transition in vitro. *Exp. Cell Res.* **335**, 187–196 (2015).

71. Hirschhaeuser, F. *et al.* Multicellular Tumour spheroids: An underestimated tool is catching up again. *J. Biotechnol.* **148**, 3–15 (2010).

72. Veelken, C., Bakker, G. J., Drell, D. & Friedl, P. Single cell-based automated quantification of therapy responses of invasive cancer spheroids in organotypic 3D culture. *Methods* **128**, 139–149 (2017).

73. Di, Z. *et al.* Ultra high content image analysis and phenotype profiling of 3D cultured micro-tissues. *PLoS One* **9**, e109688 (2014).

74. Jang, M., Yang, S. & Kim, P. Microdroplet-based cell culture models and their application. *Biochip J.* **10**, 310–317 (2016).

75. Ivascu, A. & Kubbies, M. Rapid generation of single-Tumour spheroids for high-throughput cell function and toxicity analysis. *J. Biomol. Screen.* **11**, 922–932 (2006).

76. Nunes, A. S., Barros, A. S., Costa, E. C., Moreira, A. F. & Correia, I. J. 3D Tumour spheroids as in vitro models to mimic in vivo human solid Tumours resistance to therapeutic drugs. *Biotechnol. Bioeng.* **116**, 206–226 (2019).

77. Froehlich, K. *et al.* Generation of Multicellular Breast Cancer Tumour Spheroids: Comparison of Different Protocols. *J. Mammary Gland Biol. Neoplasia* **21**, 89–98 (2016).

78. Lee, G. Y., Kenny, P. A., Lee, E. H. & Bissell, M. J. Three-dimensional culture models of normal and malignant breast epithelial cells. *Nat. Methods* **4**, 359–365 (2007).

79. Katt, M. E., Placone, A. L., Wong, A. D., Xu, Z. S. & Searson, P. C. In vitro Tumour models: Advantages, disadvantages, variables, and selecting the right platform. *Front. Bioeng. Biotechnol.* **4**, (2016).

80. Shoval, H. *et al.* Tumour cells and their crosstalk with endothelial cells in 3D spheroids. *Sci. Rep.* **7**, 1–11 (2017).

81. Truong, H. H. *et al.* Automated microinjection of cell-polymer suspensions in 3D ECM scaffolds for high-throughput quantitative cancer invasion screens. *Biomaterials* **33**, 181–8 (2012).

82. Li, Y. & Kumacheva, E. Hydrogel microenvironments for cancer spheroid growth and drug screening. *Sci. Adv.* **4**, eaas8998 (2018).

83. Ivascu, A. & Kubbies, M. *Diversity of cell-mediated adhesions in breast cancer spheroids.*

International Journal of Oncology **31**, (2007).

84. Fang, J. Y., Tan, S. J., Yang, Z., Tayag, C. & Han, B. Tumour bioengineering using a transglutaminase crosslinked hydrogel. *PLoS One* **9**, (2014).

85. Shi, W. *et al.* Facile Tumour Spheroids Formation in Large Quantity with Controllable Size and High Uniformity. *Sci. Rep.* **8**, 1–9 (2018).

86. Nath, S. & Devi, G. R. Three-dimensional culture systems in cancer research: Focus on Tumour spheroid model. *Pharmacol. Ther.* **163**, 94–108 (2016).

87. Pereira-Veiga, T. *et al.* CTCs-derived xenograft development in a triple negative breast cancer case. *Int. J. Cancer* 1–12 (2018). doi:10.1002/ijc.32001

88. Malindisa, S., Joseph, J. & Ntwasa, M. Two-Dimensional (2D) and Three-Dimensional (3D) Cell Culturing in Drug Discovery. in (2019). doi:10.5772/intechopen.81552

89. Ivanov, D. P. & Grabowska, A. M. Spheroid arrays for high-throughput single-cell analysis of spatial patterns and biomarker expression in 3D. *Sci. Rep.* **7**, 1–12 (2017).

90. Convery, N. & Gadegaard, N. 30 Years of Microfluidics. *Micro Nano Eng.* **2**, 76–91 (2019).

91. McDonald, J. *et al.* Fabrication of microfluidic systems in poly(dimethylsiloxane). *Electrophoresis* **21**, 27–40 (2000).

92. Song, H., Tice, J. D. & Ismagilov, R. F. A microfluidic system for controlling reaction networks in time. *Angew. Chemie - Int. Ed.* **42**, 768–772 (2003).

93. Joensson, H. N. & Andersson Svahn, H. Droplet microfluidics-A tool for single-cell analysis. *Angew. Chemie - Int. Ed.* **51**, 12176–12192 (2012).

94. Vitor, M. T., Casagr, C., Sipoli, e & Torre, L. G. D. La. Droplet-based Microfluidic Systems for Production and Transfection InVitro of Non-Viral Vectors for Gene Delivery. *Res. Rev. J. Pharm. Pharm. Sci.* **4**, 1–17 (2015).

95. Mashaghi, S., Abbaspourrad, A., Weitz, D. A. & van Oijen, A. M. Droplet microfluidics: A tool for biology, chemistry and nanotechnology. *TrAC - Trends Anal. Chem.* **82**, 118–125 (2016).

96. Huebner, A. *et al.* Microdroplets: A sea of applications? *Lab Chip* **8**, 1244–1254 (2008).

97. Zhang, Y. S., Zhang, Y. N. & Zhang, W. Cancer-on-a-chip systems at the frontier of nanomedicine. *Drug Discov. Today* **22**, 1392–1399 (2017).

98. Chen, P., Feng, X., Du, W. & Liu, B. F. Microfluidic chips for cell sorting. *Front. Biosci.* **13**, 2464–2483 (2008).

99. Teixeira, A. *et al.* Microfluidics-Driven Fabrication of a Low Cost and Ultrasensitive SERS-Based Paper Biosensor. *Appl. Sci.* **9**, 1387 (2019).

100. Kevin Oliveira, Alexandra Teixeira, Claudia Lopes, Jose Maria Fernandes, Paulina Piairo, Lei Wu, L. D. & Abalde-Cela, S. SERS phenotyping of single cancer cells in microdroplets. *Manuscr. Prep.* (2019).

101. Hayat, Z. & El Abed, A. I. High-throughput optofluidic acquisition of microdroplets in microfluidic systems. *Micromachines* **9**, (2018).

102. Ward, T., Faivre, M., Abkarian, M. & Stone, H. A. Microfluidic flow focusing: Drop size and scaling in pressure versus flow-rate-driven pumping. *Electrophoresis* **26**, 3716–3724 (2005).

103. Mavrogiannis, N., Ibo, M., Fu, X., Crivellari, F. & Gagnon, Z. Microfluidics made easy: A robust low-cost constant pressure flow controller for engineers and cell biologists. *Biomicrofluidics* **10**, 1–12 (2016).

104. Kaminski, T. S., Scheler, O. & Garstecki, P. Droplet microfluidics for microbiology: Techniques, applications and challenges. *Lab Chip* **16**, 2168–2187 (2016).

105. Jiu-Sheng, C. & Jia-Huan, J. Droplet microfluidic technology: Mirodroplets formation and

manipulation. *Fenxi Huaxue/ Chinese Journal of Analytical Chemistry* **40**, 1293–1300 (2012).

106. Gu, H., Duits, M. H. G. & Mugele, F. Droplets formation and merging in two-phase flow microfluidics. *Int. J. Mol. Sci.* **12**, 2572–2597 (2011).

107. Baroud, C. N., Gallaire, F. & Dangla, R. Dynamics of microfluidic droplets. *Lab Chip* **10**, 2032–2045 (2010).

108. Lapierre, F., Wu, N. & Zhu, Y. Influence of flow rate on the droplet generation process in a microfluidic chip. *Smart Nano-Micro Mater. Devices* **8204**, 82040H (2011).

109. Lee, W., Walker, L. M. & Anna, S. L. Role of geometry and fluid properties in droplet and thread formation processes in planar flow focusing. *Phys. Fluids* **21**, (2009).

110. Collins, J. & Lee, A. P. Control of serial microfluidic droplet size gradient by step-wise ramping of flow rates. *Microfluid. Nanofluidics* **3**, 19–25 (2007).

111. Loizou, K., Wong, V. L. & Hewakandamby, B. Examining the effect of flow rate ratio on droplet generation and regime transition in a microfluidic t-junction at constant capillary numbers. *Inventions* **3**, (2018).

112. Hymel, S. J., Lan, H., Fujioka, H. & Khismatullin, D. B. Cell trapping in Y-junction microchannels: A numerical study of the bifurcation angle effect in inertial microfluidics. *Phys. Fluids* **31**, 082003 (2019).

113. Lagus, T. P. & Edd, J. F. High-throughput co-encapsulation of self-ordered cell trains: Cell pair interactions in microdroplets. *RSC Adv.* **3**, 20512–20522 (2013).

114. Li, L. *et al.* Dean Flow Assisted Single Cell and Bead Encapsulation for High Performance Single Cell Expression Profiling. *ACS Sensors* **4**, 1299–1305 (2019).

115. Buryk-Iggers, S., Kieda, J. & Tsai, S. S. H. Diamagnetic droplet microfluidics applied to single-cell sorting. *AIP Adv.* **9**, (2019).

116. Abalde-Cela, S., Taladriz-Blanco, P., De Oliveira, M. G. & Abell, C. Droplet microfluidics for the highly controlled synthesis of branched gold nanoparticles. *Sci. Rep.* **8**, 1–6 (2018).

117. Jo, Y., Shen, F., Hahn, Y. K., Park, J. H. & Park, J. K. Magnetophoretic sorting of single cell-containing microdroplets. *Micromachines* **7**, 1–9 (2016).

118. Best, R. J. *et al.* Label-Free Analysis and Sorting of Microalgae and Cyanobacteria in Microdroplets by Intrinsic Chlorophyll Fluorescence for the Identification of Fast Growing Strains. *Anal. Chem.* **88**, 10445–10451 (2016).

119. Yu, L. *et al.* Core-shell hydrogel beads with extracellular matrix for Tumour spheroid formation. *Biomicrofluidics* **9**, 1–12 (2015).

120. Kang, D. K., Monsur Ali, M., Zhang, K., Pone, E. J. & Zhao, W. Droplet microfluidics for single-molecule and single-cell analysis in cancer research, diagnosis and therapy. *TrAC - Trends Anal. Chem.* **58**, 145–153 (2014).

121. Kim, P. *et al.* Soft lithography for microfluidics: a review. *Biochip J.* **2**, 1–11 (2008).

122. Datar, A., Joshi, P. & Lee, M. Y. Biocompatible hydrogels for microarray cell printing and encapsulation. *Biosensors* **5**, 647–663 (2015).

123. Johari, S. *et al.* The effect of softbaking temperature on SU-8 photoresist performance. *IEEE Int. Conf. Semicond. Electron. Proceedings, ICSE* 467–470 (2014). doi:10.1109/SMELEC.2014.6920899

124. Theberge, A. B. *et al.* Microdroplets in microfluidics: An evolving platform for discoveries in chemistry and biology. *Angew. Chemie - Int. Ed.* **49**, 5846–5868 (2010).

125. Moon, S. J., Ceyhan, E., Gurkan, U. A. & Demirci, U. Statistical modeling of single target cell encapsulation. *PLoS One* **6**, (2011).

126. Collins, D. J., Neild, A., deMello, A., Liu, A. Q. & Ai, Y. The Poisson distribution and beyond: Methods for microfluidic droplet production and single cell encapsulation. *Lab Chip* **15**, 3439–3459 (2015).

127. Hu, R. *et al.* Encapsulation of single cells into monodisperse droplets by fluorescence-activated droplet formation on a microfluidic chip. *Talanta* **153**, 253–259 (2016).

128. Eddings, M. A., Johnson, M. A. & Gale, B. K. Determining the optimal PDMS-PDMS bonding technique for microfluidic devices. *J. Micromechanics Microengineering* **18**, (2008).

129. Vemuri, S. K. *et al.* Novel biosynthesized gold nanoparticles as anti-cancer agents against breast cancer: Synthesis, biological evaluation, molecular modelling studies. *Mater. Sci. Eng. C* **99**, 417–429 (2019).

130. Hagemann, J. *et al.* Therapy Testing in a Spheroid-based 3D Cell Culture Model for Head and Neck Squamous Cell Carcinoma. *J. Vis. Exp.* (2018). doi:10.3791/57012

131. Arnoletti, J. P. *et al.* Pancreatic and bile duct cancer circulating Tumour cells (CTC) form immune-resistant multi-cell type clusters in the portal venous circulation. *Cancer Biol. Ther.* **19**, 887–897 (2018).

132. Merkel, T. C., Bondar, V. I., Nagai, K., Freeman, B. D. & Pinnau, I. Gas Sorption, Diffusion, and Permeation in Poly(dimethylsiloxane) The permeability of poly(dimethylsiloxane) [PDMS] to. *J Polym Sci B Polym Phys* **38**, 415–434 (2000).

133. Xu, W. *et al.* A vapor based microfluidic flow regulator. *Sensors Actuators, B Chem.* **142**, 355–361 (2009).

134. Bao, F. B., Lin, J. Z. & Shi, X. Simulation of gas flow and heat transfer in micro Poiseuille flow. *3rd IEEE Int. Conf. Nano/Micro Eng. Mol. Syst. NEMS* **51**, 103–107 (2008).
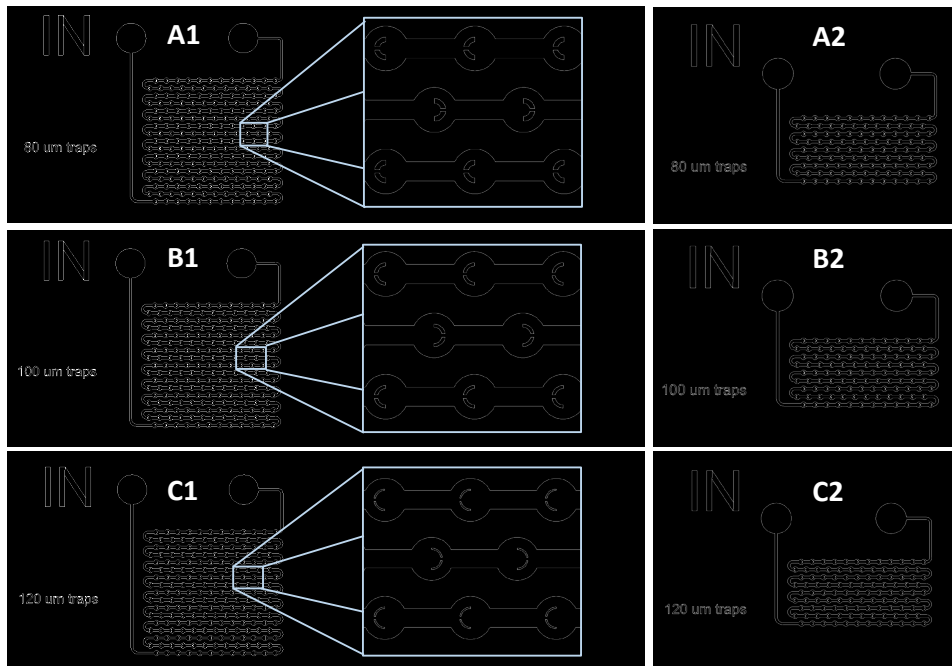
Annex 1 – Master mould designs (Gen. 3)

Figure 21 - AutoCAD designs of the Gen. 3 reservoirs: 80 µm circular traps, with 17 (A1) and 9 (A2) rows, 100 µm circular traps, with 17 (B1) and 9 (B2) rows and 120 µm circular traps, with 17 (C1) and
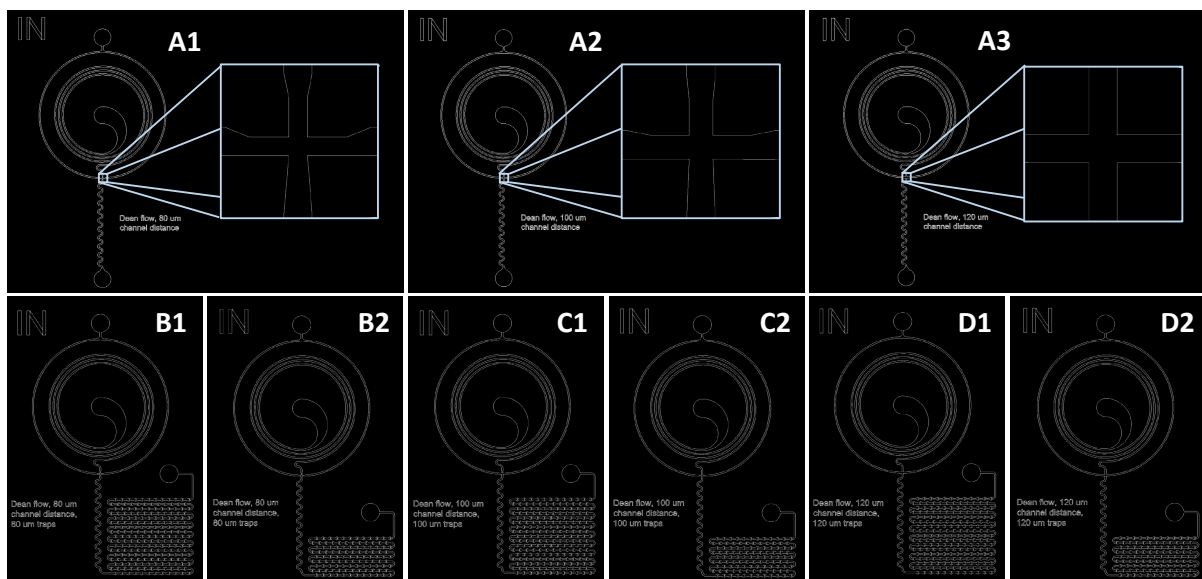

Figure 22 - AutoCAD designs of the Gen. 3 droplet generators: 80 µm width T-section (A1), 100 µm width T-section (A2) and 120 µm width T-section (A3). AutoCAD designs of the Gen. 3 combined mould devices: 80 µm width T-section and trap size with 17 rows (B1) and 9 rows (B2), 100 µm width T-section and trap size with 17 rows (C1) and 9 rows (C2) and 120 µm width T-section and trap size with 17 rows (D1) and 9 rows (D2), having each row 12 traps in line.
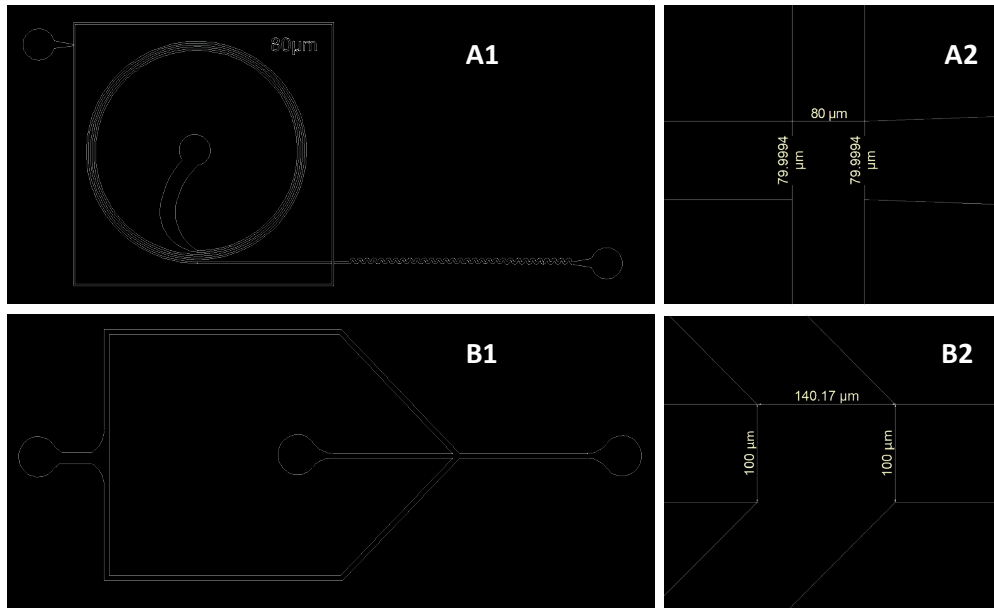
Annex 2 – Gen. 1 and Gen. 2 devices

Figure 23 – Gen. 2 AutoCAD designs of the Dean flow droplet generator (A1) with 80 µm width T-section (A2) and Gen. 1 AutoCAD designs of the flow-focusing droplet generator (B1) with 100 µm width T-section (B2)
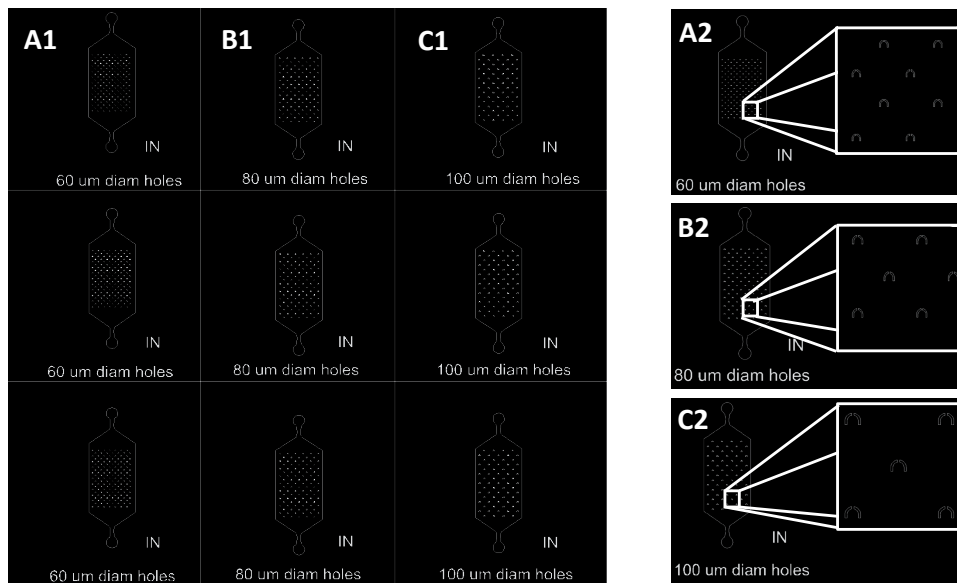

Figure 24 - Gen. 1 AutoCAD designs of trap reservoirs with trap widths of 60 µm (A1), 80 µm (B1) and 120 µm (C1), also with amplifications of the spacing of the traps for the 60 µm (A2), 80 µm (B2) and 120 µm (C2) trap reservoirs.
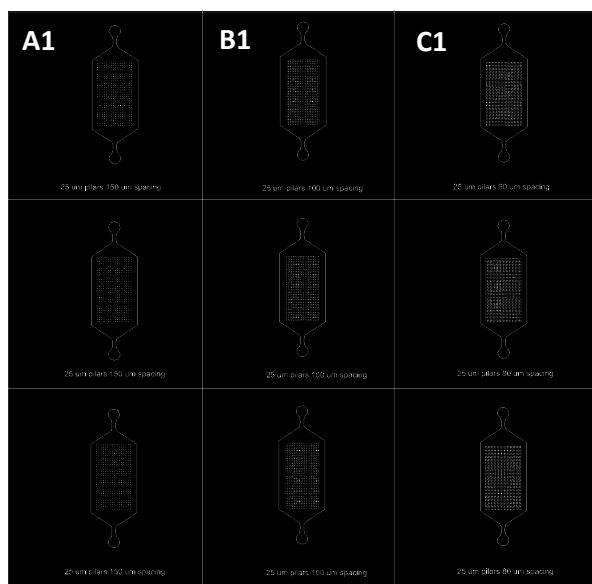
Figure 25 - Gen. 1 AutoCAD design of 25 µm diameter pillar reservoirs with spacing between pillars of 150 µm (A1), 100 µm (B1) and 80 µm (C1).
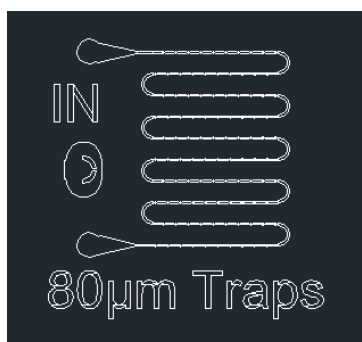

Figure 26 - AutoCAD Gen.2 linear reservoirs design.

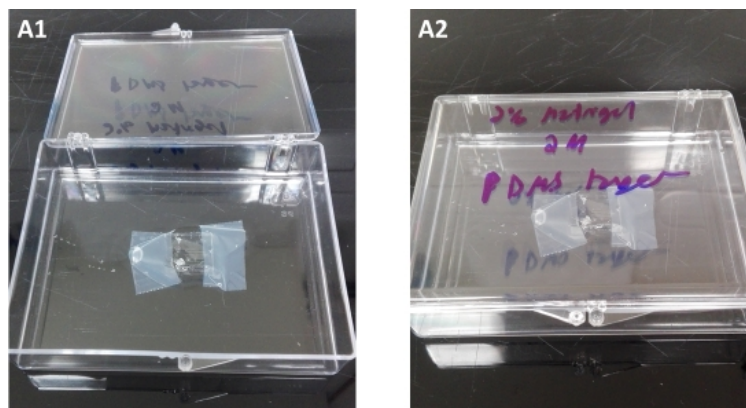# Annex 3 – Live pictures depicting actual experimental conditions

Figure 27 - Illustrative figure that represents the conditions of the device after the preparation process for the incubator, with open lid (A1) for extraction and placement of the reservoir and closed lid (A2) for placement in incubator.

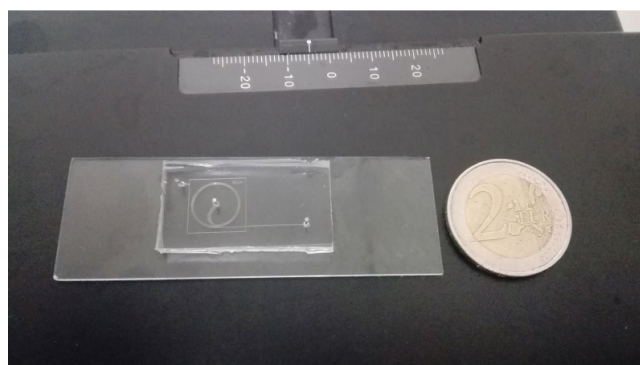*Figure 28 - Image of the hemocytometer used for cell count.*

Figure 29 – Comparative picture of the size of the devices to a 2€ coin.
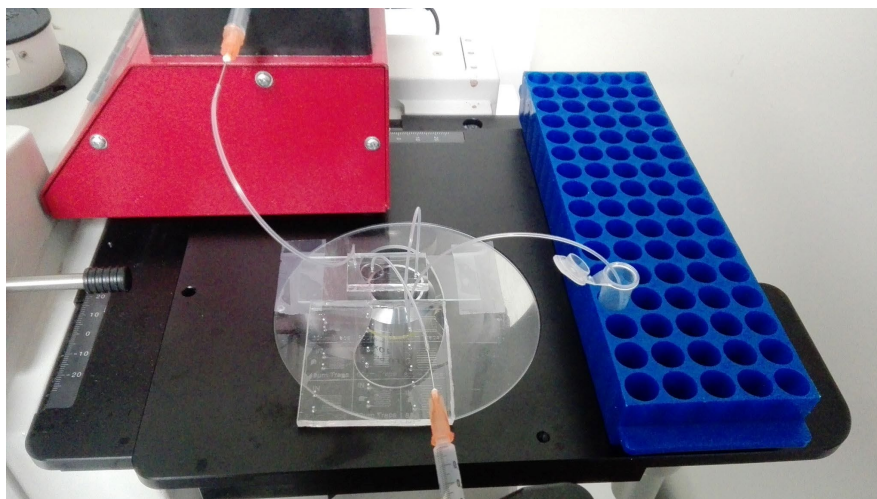
Figure 30 – Image depicting the actual aspect of the cell encapsulation experiments.

Annex 4 – Profilometer results
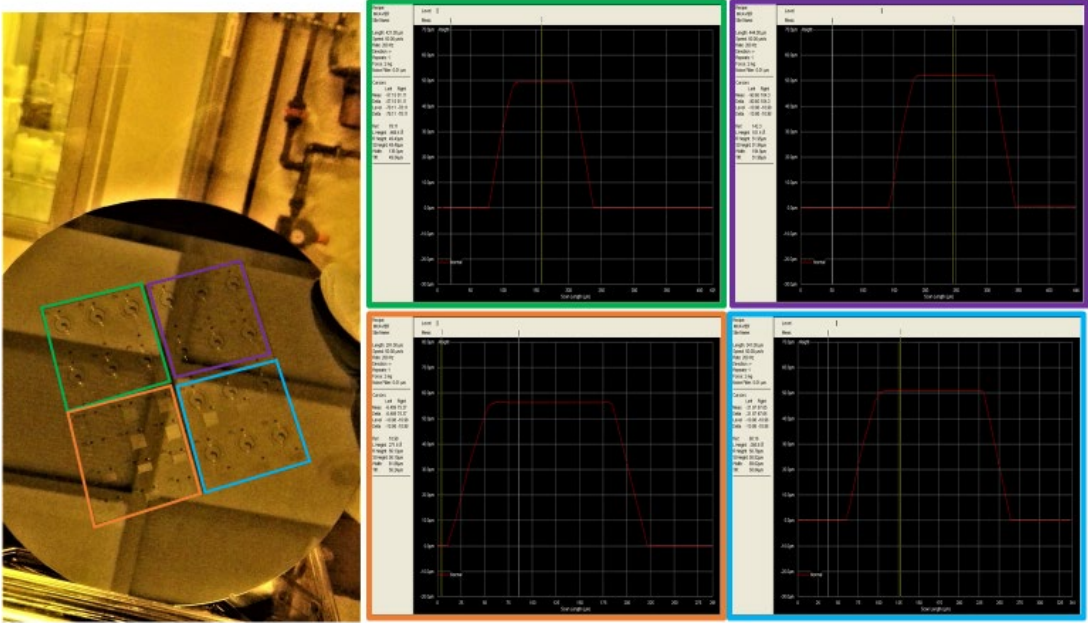
Figure 31 - Results of the profilometer readings for each section of the wafer (A): (B) - Top left; (C) - Top right; (D) - Bottom left; (E) – Bottom right.

Annex 5 – Average droplet size calibration results (Gen. 1 and Gen. 2)

Figure 32 - Picture capture of the microdroplet samples produced by Gen. 1 (A) and Gen. 2 (B) using Milli-Q as the dispersive phase and FC-40 + Pico-Surf™ 1 (PS-1) as the continuous phase, followed with a subsequent analysis regarding average size, and size dispersion with different ratio values between the continuous and dispersive phases of 25 (A1), 20 (B1), 10 (A2, B2), 5 (A3, B3) and 2.5 (A4).

Annex 6 – Different types of sealing method results

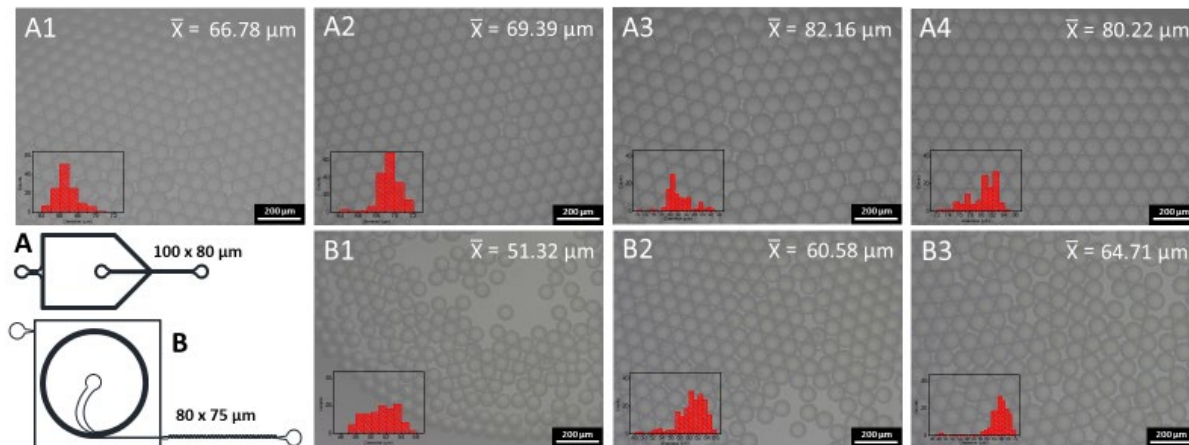- In the initial stages of the thesis, using the burning tips technique for sealing the reservoirs was not efficient, having several experiments compromised after 2 days. To that end, a new method of sealing was researched, eventually deciding on a method that takes advantage of the inherent abilities of the liquid cross-linked PDMS to solidify at room temperature. The idea consisted in pouring liquid cross-linked PDMS onto the opening at the inlets of the reservoirs, after removing the LDPE tubing entirely from the inlets. For this method to work, the liquid PDMS had to be degassed previously and poured almost immediately over the inlets. Figure 15 represents the first experiment using this method with HFE 7500 + PS-1 as the continuous phase. Figure 16 represents a second experiment using this method and the burning tips technique in two different reservoirs for comparison, with FC-40 + PS-1 as the continuous phase.

- The results from Figure 15 appear to confirm that the introduction of FC-40 as the continuous phase helps in limiting the entrance of air in the devices through the inlets. However, based on the contradictory results shown in Figure 16, the sealing method by solidifying PDMS in the inlets does not appear to be as efficient as predicted, so, that technique will have to be studied more before it can be used for further experiments[132]. Also, the technique involving the "burned tips" appears to require more hands-on experience by the user to be properly efficient.

- Based on all the previous results for the sealing experiments, the best combination of experimental settings that may augment the stability of microdroplets for long-term observation reside with the continuous use of FC-40 as the continuous phase and, while the sealing method still depends on the skill of the user, the method of the "burning tips" may remain the most facile way of sealing the reservoirs immediately. However, as the images can demonstrate, with the passage of days, the evaporation of liquid and subsequent diffusion into the PDMS material starts to produce "haze", which complicated the observation of microdroplets for long periods of time. To that end, it may be required to study the possibility of changing the bottom layer of the device.
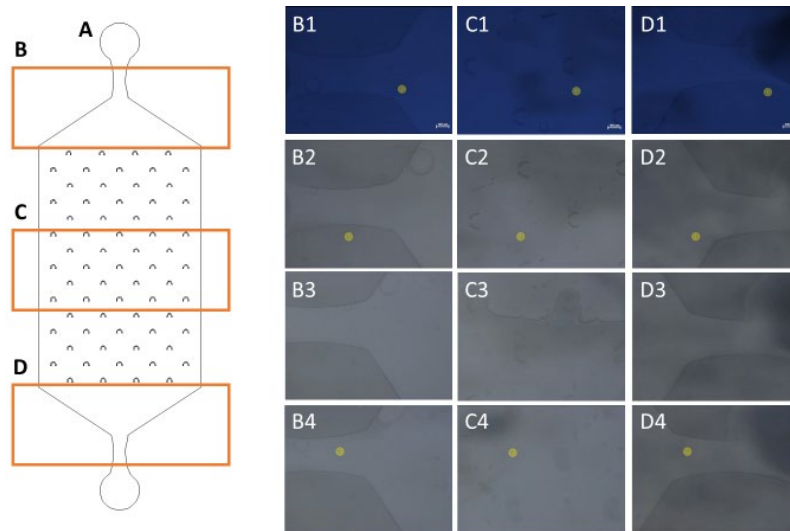
Figure 33 - Results of the encapsulation and weekly observation of the closing of the Gen. 1 reservoirs with 100 µm traps (A), using Milli-Q as the dispersive phase and HFE 7500 + PS-1 as the continuous phase, in three specific regions: upper inlet (B), middle (C) and lower inlet (D). The pictures of the experiment were taken within four time periods: day 1 (B1, C1, D1), day 7 (B2, C2, D2), day 15 (B3, C3, D3) and day 21 (B4, C4, D4).
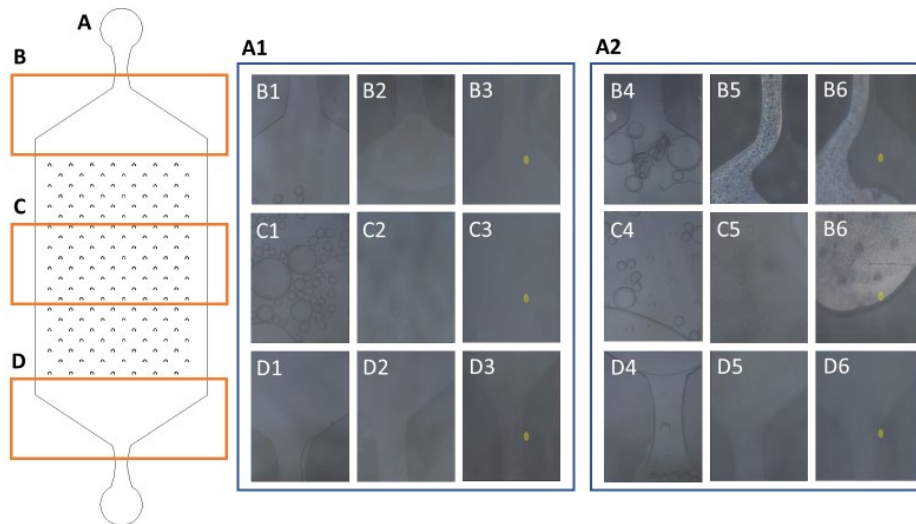
Figure 34 - Results of the encapsulation and daily observation of the closing of the two Gen. 1 reservoirs with 60 µm traps (A) for the comparison experiment between the two sealing methods of "burning tips" (A1) and "liquid PDMS pouring" (A2) in three specific regions: upper inlet (B), middle (C) and lower inlet (D). The pictures of the experiment were taken within three time periods: day 1 (B1-B6), day 7 (C1-C6) and day 15 (D1-D6). The continuous phase used was FC-40 + PS-1 and the dispersive phase used was Milli-Q.

- An alternative method of sealing the devices and ensuring the flow of the liquid passing through the channels was formulated, using the inherent property of gasses in expanding and contracting based on the room temperature[133,134]. A figure exemplifying a possible setup of that method is illustrated in Figure 31, Annex 6. Initial results indicated that, while the liquid was kept in motion within the reservoir, the trajectory was never in the same direction, making the microdroplets avoid the traps. The alternative method had to be abandoned due to an abundance of complications.
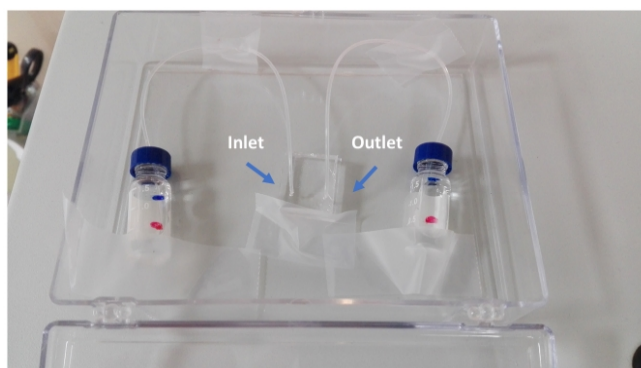
Figure 35 - Illustration of the alternative sealing method. The idea consisted in a difference of height between the liquid in both bottles (which was FC-40) being pushed through the channel without external assistance, with the inlet being connected to the bottle with the least liquid and the outlet connected to the bottles with the most liquid, as measured by the blue marks on the bottles. The red marks indicated the height at which the LDPE tubing was put which was the same height for both bottles, in order to balance out the pressure exercised on the liquid entering the tubing.

Annex 7 – Pictures of samples for the cell encapsulation experiment
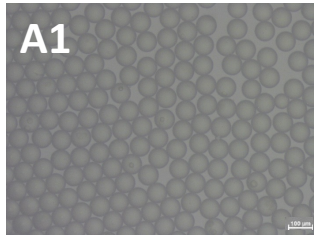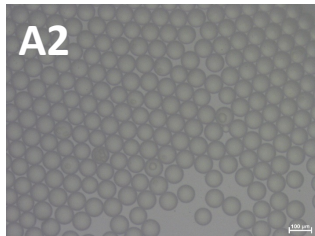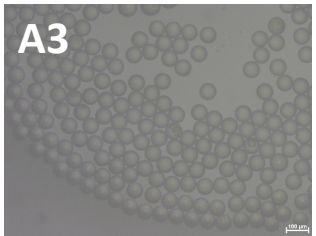
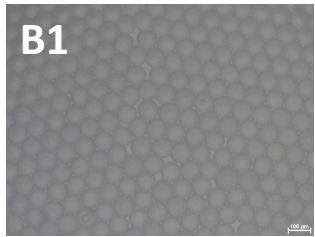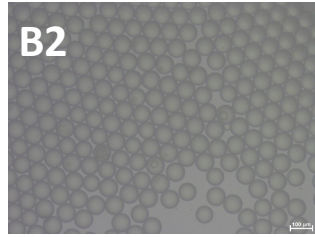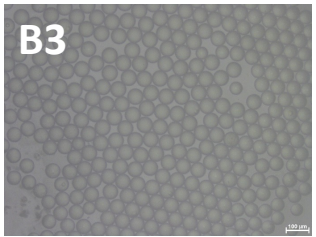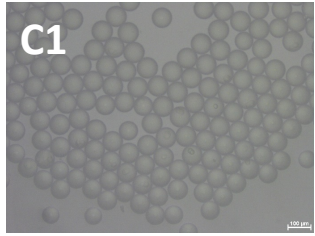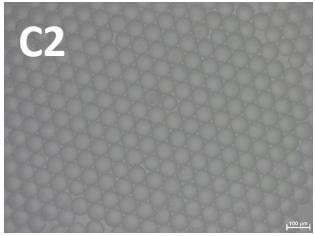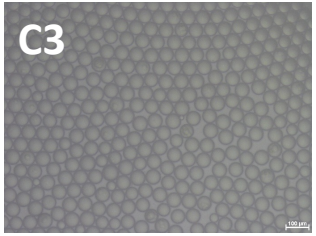|	$Q_{disp.}$		
Cell type/ ρ	500	1000	2000
MDA 1M	A1	A2	A3
SK-BR-3 2M	B1	B2	B3
SK-BR-3 3M	C1	C2	C3

Figure 36 – Pictures used to extrapolate the values of the encapsulation rates for the experiment in Chapter 3.4.

Annex 8 – Table for the design of the cell culture conditions in microdroplets

Table 10 - Complete table off the articles used to develop the cell culture method used.

Reference	Cell line	Stating n cells	Method	Culture media	Matrix	Volume	Incubating conditions	Time to grow	Growth dynamics
83	MDA-MB-435 S/SK-BR-3	3000000	96-well plates	RPMI-1640 supplemented with 10% FCS and 2 mM L-Glutamine	2,5% rBM	200 µL	37 ºC 7% CO2	24h	Within 24h (not specified if they did intermediate observations)
77	MCF-7	10000	Hanging drop	DMEM with high glucose and 25% methocel and 10 % FCS	1% Matrigel	20 µL each	37 ºC 5% CO2	3 days	3 days to obtain results, plus 6h to analyse morphology and 48h for colapse
84	MDA-MB-231	100000	48-well plates	DMEM with 10 % FBS and 1% Penicillin/Streptomycin	Col-Tgel (defined by droplet size)	20 µL for 40000 cells	37 ºC	6 days	Observations performed at day 0, 2 ,4 and 6
81	MDA-MB-231	5000	96-well plates	10 ml DMEM, then added 0.75% agarose	Collagen type I Gel dilluted to 2.4 mg/ml in PBS containing 1xDMEM, 44 mM NaHCO3, 0.1 M Hepes	20 µL	37 ºC 5% CO2	24h + 48h	24h for aggregates, 48 h for spheroids
72	MV3-melanoma	4000	hanging drop	DMEM, supplemented with 10% FCS, penicillin 100 U/ml and streptomycin 100mg/ml, L-glutamine 2 mM, and sodium pyruvate 1 mM	Methylcellulose with concentration of 4.8 mg/ml and diluted bovine dermis collagen I solution with a final concentration of 10 mg/ml, for a cell concentration of 1.67 x 10^5 cells/ml	30 µL	37 ºC 5% CO2	24h	24h to form spheroids, with an extended incubation period for 30h as optional, and 24h after spheroid formation, the sphe-

									roids developped hypoxia
119	MCF-7	1 or more cells, cannot specify because the project did not try to ensure single cell encapsulation	Droplet encapsulation, with a distinct barrier between the bead and the spheroid medium	RPMI media with 10% FBS and 1% penicillin/streptomycin	100 µL of collagen I at a concentration of 9.21 mg/ml, 200 µL of MatrigelVR was added and mixed with the collagen, 5 µL NaHCO3 to reach pH 7.3–7.5. 50 µL of MCF-7 cells in PBS and 250 µL of 2% Manucol LKX alginate	126 pL, after calculating volume from 311.68 µm	37 ºC 5% CO2	Not specified, stablishes timelines based on core components, from 2 to 4 days	Follows a linear trend with alginate, but starts to increase with addition on collagen and Matrigel, up to 1.5x the original ratio of proliferation
129	MCF-7 and MDA-MB-231	300000	Aseptically cultured in T-25 cell culture flasks/multi-well cell culture plates	Hi-Gluta XL™ Dulbecco's Modified Eagle's Medium (DMEM) (High Glucose), supplemented with 10% fetal bovine serum, 50 units/mL penicillin, and 50 µg/mL streptomycin	Cultured onto 1.2% agarose-coated 96-well plates	Not specified	Not specified	4 days (24h + 24h + 48h)	24h for seeding, plus 24h for culture and 48h for spheroid formation
130	Head and Neck squamous cell carcinoma (HNSCC) extracted from patients	5000 primary cells, or 1000-2000 intermediary cells	96-well plates	equal parts DMEM and airway epithelial cell medium (BEGM), 10% fetal bovine serum,1% penicillin/streptomycin, 1% sodium pyruvate, 1% non-essential amino acids, 1% L-glutamin	Not specified	300-400 µL	37 ºC 5% CO2	7-10 days	Change media every 24h, until spheroid growth is confirmed
131	Peripheral blood mononuclear cells (PoBMC)	1000000 - 5000000	48 or 96-well plates	RPMI 1640,10% medium 199, 10% fetal calf serum, 2% antibiotic-anti-mycotic mix	10 µg/ml fibronectin, 10µg/ml adiponectin, 0.5µg/ml MCSF or 50% Matrigel	Not specified	Starts at 37 ºC 7% CO2, but after the clusters are formed, they are cryogenically	7 days, re-supplied with media each 3 days	Cell clusters appear after 7 days, but they are left to grow for 21 days

							pre-served at -80ºC	
69	Human prostate cancer cell lines PC3 and LnCAP, human breast cancer cell lines MDA-MB-231 and MCF-7, and lung cancer cell line H460	Not specified	100-mm Petri Dishes	PC3 and LnCAP cells were grown in (RPMI-1640) culture medium (2 mM glutamine, +sodi-umpyruvate) supplemented with 10% fetalbovine serum. MCF-7 and MDA-MB-231 cells were grown in (DMEM) high glucose (4500 mg/L glucose; 4 mM glutamine, + sodium pyruvate) supplemented with 10% FBS. H460 cells were grown in RPMI-1640 culture medium supplemented with 5% FBS. All media were supplemented with 100 U/ml penicillin and 100 mg/ml streptomycin.	Media used in each cell line in a 100-mm Petri dish coated with Poly-HEMA, each with 15 mL of each media	15 mL	37 ºC 5% CO_2	Over 7 days	Complete media is replaced twice a week for mainte-nance
24	Head neck cancer cells extracted from patients	Not specified	96-well standard micro-plates, 96F non-adher-ent micro-plates, spheroid microplates and specialized microwell formats	DMEM/F12 with additives; 50 ng/mL EGF, 5% v/v R-spondin 1, 10% v/v Noggin, 10 ng/mL FGF10, 1 ng/ml FGF2, 10 nM Nicotinamide, 0.5 µM A83–01, 10 µM SB202190, 10 µM Y-27632, 1X B27 Additive, 1.25 mM N-Ace-tyl-L-cysteine, 2 nM Glutamax, 10 mM HEPES, 1:100 v/v Pri-mocin	Happy Cell hydrogel with the media previously mentioned	10 mL	37 ºC 2% O_2, 5% CO_2	Esti-mated time of 7 days	Not speci-fied

Annex 9 – Summary of the experiments and examples of compilations of pictures into reservoirs

For the duration of the thesis, during the cell encapsulation and monitoring stage, a total of 46 reservoirs were filled and sealed, based on the number of sets, the defining characteristic for observation in each set, how many variations of that characteristic existed to test in each set and the existence of one replica per each reservoir made. Table 11 contains a count of the total number of reservoirs per each set and how many were considered stable enough for further analysis.

Table 11 – Summary of the total number of filled reservoirs per each set and the number of sets viable for detailed analysis.

Sets	Number of reservoirs prepared	Number of reservoirs viable after preparation
1	7	7
2	3	3
3	8	8
4	16	15
5	12	9

Since the only characterization technique available was optical microscopy, is was not possible to confirm the contents of the microdroplets, mainly regarding the presence of Matrigel® within the microdroplets and if the cellular-shaped figures that appear inside the microdroplets are indeed the cancer cells that were placed in the dispersive phase solution. Air bubbles tend to be formed due to incomplete removal of air from the syringes, and they can be confused for cells if they have a similar size. One way to distinguish cell from air bubbles resided in their difference in optical properties regarding light refraction and diffraction. Using dark field visualization settings, it was possible to see which cell-shaped objects could allow the passage of light without significant deviation, allowing to remove air bubbles from total cell count as false positives.

Below are three examples of complete collages of pictures to illustrate the process of monitorization from day 0 to the final observation available (Figures 37 and 38) and to demonstrate the differences between the theoretical counting and the experimental counting when dealing with high numbers of microdroplets (Figure 39, Tables 15, 16 and 17).
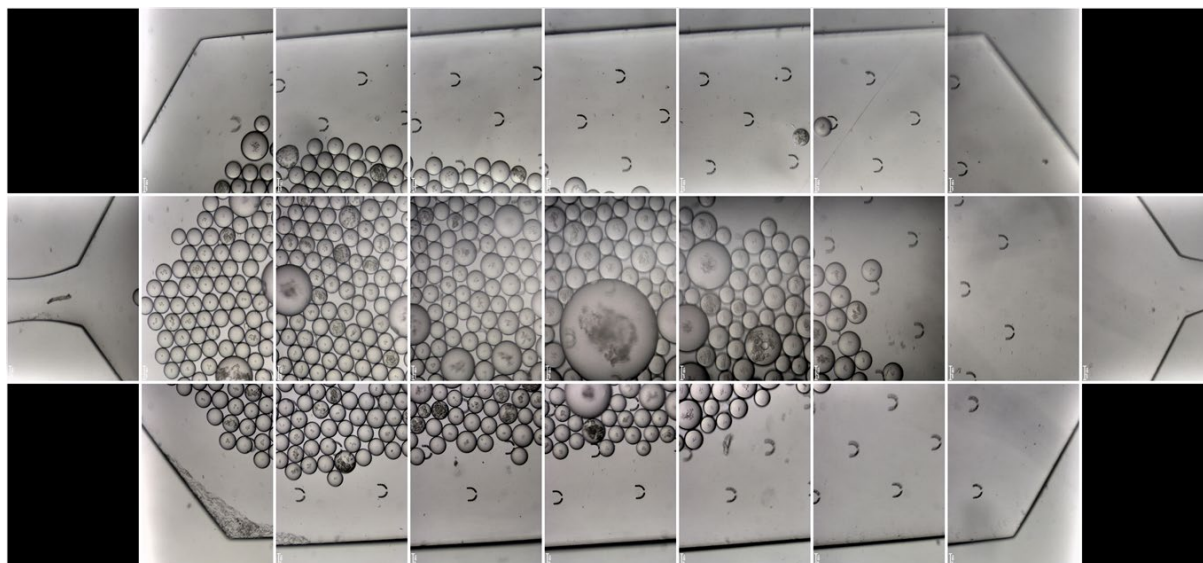
Figure 37 - Collage of 23 optical microscope pictures of a sealed PDMS wide reservoir with microdroplets encapsulated with MDA-MB-435 cells, with a cell density of 2 × 10⁶ cells mL⁻¹, 8 % Matrigel concentration and PDMS bottom layer, monitored right after microdroplet generation, from the 4ᵗʰ set of experiments.

Table 12 - Values obtained for diameter estimates about average, standard deviation, maximum and minimum from analysing the counted number of microdroplets in the picture captions from reservoir 2 with PDMS bottom layer right after sealing the reservoir.

Number of microdroplets counted	Diameter average (µm)	Diameter Standard Deviation (µm)	Diameter (Max) (µm)	Diameter (Min) (µm)
375	113.94	15.41	181.55	89.45

Table 13 - Calculation of the theoretical results for cell encapsulation in microdroplets, depending on the estimated cell density and the average diameter calculated previously.

Diameter average (µm): 113.94	Empty microdroplets	Nº of microdroplets with 1 cell	Nº of microdroplets with 2 cells	Nº of microdroplets with 3 cells	Nº of microdroplets with 4 cells	Nº of microdroplets with 5 cells	Nº of microdroplets with 6 or more cells
	80	123	96	49	19	6	2
Ratio (%)	21.25	32.91	25.49	13.16	5.10	1.58	0.52

Table 14 – Results from counting the contents of each microdroplet present in reservoir 2 with PDMS bottom layer right after sealing the reservoir, with the ratio calculated for each partition of the microdroplets when comparing to the total of microdroplets counted.

Experimental values							
Number of micro-droplets counted: 375	**Empty micro-droplets**	**Nº of mi-cro-droplets with 1 cell**	**Nº of mi-cro-droplets with 2 cells**	**Nº of micro-droplets with 3 cells**	**Nº of micro-droplets with 4 cells**	**Nº of micro-droplets with 5 cells**	**Nº of mi-cro-droplets with 6 or more cells**
	76	59	63	32	26	8	111
Ratio (%)	20.27	15.73	16.80	8.53	6.93	2.13	29.60

Figure 38 - Collage of 23 microscope pictures of a sealed PDMS wide reservoir with microdroplets encapsulated with MDA-MB-435 cells, with a cell density of 2×10^6 cells mL^{-1}, 8 % Matrigel concentration and PDMS bottom layer, monitored 360 h after microdroplet generation, from the 4th set of experiments.
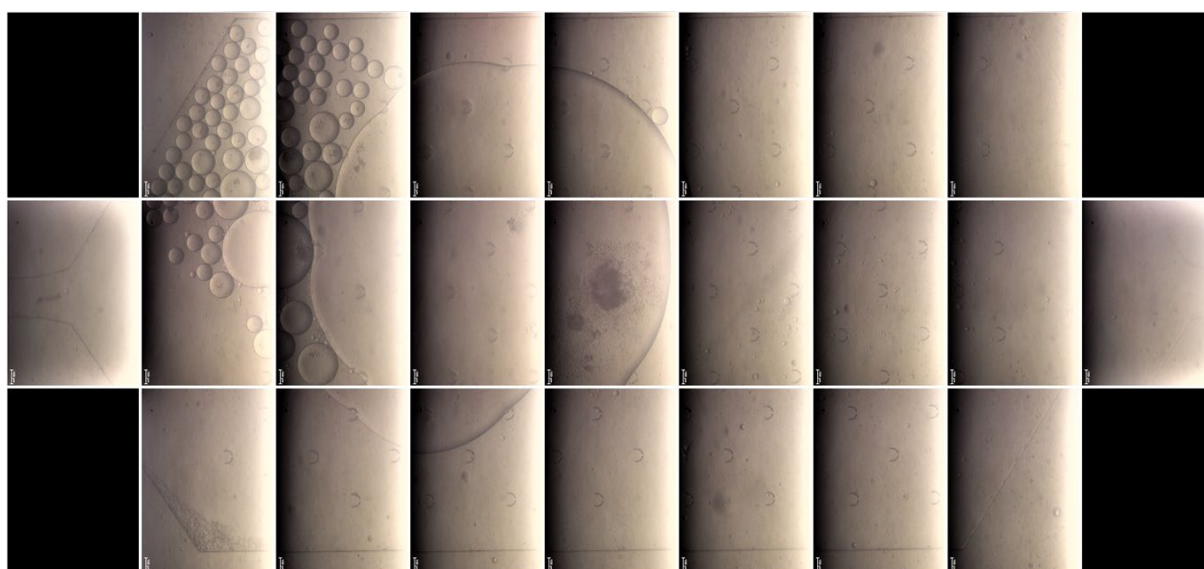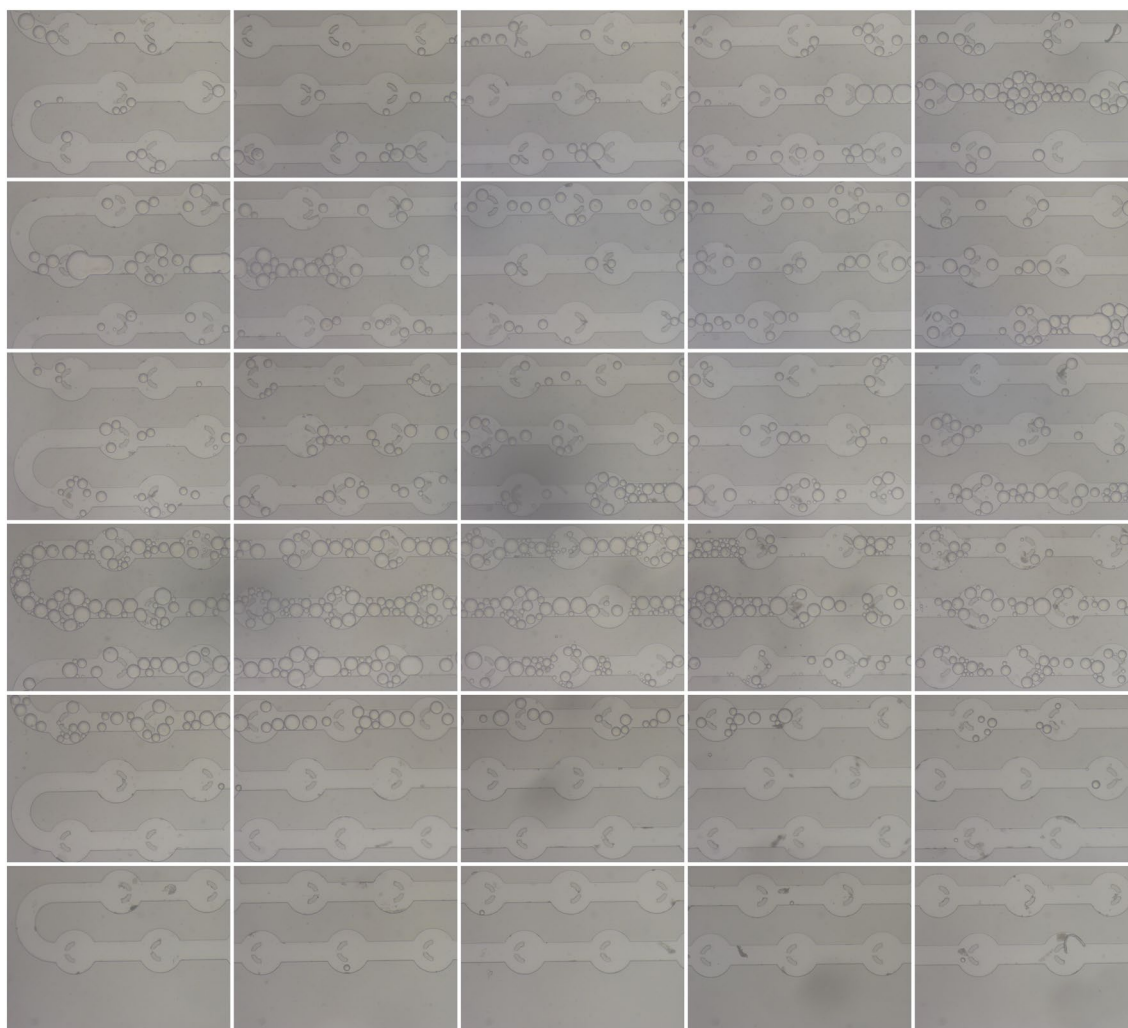
Figure 39 - Collage of 30 microscope pictures of a sealed PDMS linear reservoir with microdroplets encapsulated with MDA-MB-435 cells, with a cell density of 1 × 10⁶ cells mL⁻¹ and 4 % Matrigel concentration, monitored right after microdroplet generation, from the 2ⁿᵈ set of experiments.

Table 15 - Values obtained for diameter estimates about average, standard deviation, maximum and minimum from analysing the counted number of microdroplets in the picture captions from reservoir 1 with 1 × 10⁶ cells mL⁻¹ cell density right after sealing the reservoir.

Number of micro-droplets counted	Diameter average (µm)	Diameter Standard Deviation (µm)	Diameter (Max) (µm)	Diameter (Min) (µm)
726	55.59	12.81	101.77	37.55

Table 16 - Calculation of the theoretical results for cell encapsulation in microdroplets, depending on the estimated cell density and the average diameter calculated previously.

Theoretical values (726 microdroplets)							
Diameter average (μm): 55.59	**Empty microdroplets**	**Nº of microdroplets with 1 cell**	**Nº of microdroplets with 2 cells**	**Nº of microdroplets with 3 cells**	**Nº of microdroplets with 4 cells**	**Nº of microdroplets with 5 cells**	**Nº of microdroplets with 6 or more cells**
	664	60	3	0	0	0	0
Ratio (%)	91.40	8.22	0.37	0.01	0.00	0.00	0.00

Table 17 – Results from counting the contents of each microdroplet present in reservoir 1 with 1×10^6 cells mL^{-1} cell density right after sealing the reservoir, with the ratio calculated for each partition of the microdroplets when comparing to the total of microdroplets counted.

Experimental values							
Number of microdroplets counted: 726	**Empty microdroplets**	**Nº of microdroplets with 1 cell**	**Nº of microdroplets with 2 cells**	**Nº of microdroplets with 3 cells**	**Nº of microdroplets with 4 cells**	**Nº of microdroplets with 5 cells**	**Nº of microdroplets with 6 or more cells**
	650	56	10	3	4	2	1
Ratio (%)	89.53	7.71	1.38	0.41	0.55	0.28	0.14